CELL MIGRATION

Atypical CXCL12 signaling enhances neutrophil migration by modulating nuclear deformability

Bianca Calì[1,2,3]*†, Mathieu Deygas[3,4], Fabio Munari[1,2], Elisabetta Marcuzzi[1,2], Antonino Cassará[2], Lara Toffali[5], Massimo Vetralla[6,7], Mathilde Bernard[3,4], Matthieu Piel[3,4], Onelia Gagliano[6,7], Marta Mastrogiovanni[8,9], Carlo Laudanna[5], Nicola Elvassore[6,7], Barbara Molon[1,2,6], Pablo Vargas[3,4,10]*‡, Antonella Viola[1,2]*‡

To reach inflamed tissues from the circulation, neutrophils must overcome physical constraints imposed by the tissue architecture, such as the endothelial barrier or the three-dimensional (3D) interstitial space. In these microenvironments, neutrophils are forced to migrate through spaces smaller than their own diameter. One of the main challenges for cell passage through narrow gaps is the deformation of the nucleus, the largest and stiffest organelle in cells. Here, we showed that chemokines, the extracellular signals that guide cell migration in vivo, modulated nuclear plasticity to support neutrophil migration in restricted microenvironments. Exploiting microfabricated devices, we found that the CXC chemokine CXCL12 enhanced the nuclear pliability of mouse bone marrow–derived neutrophils to sustain their migration in 3D landscapes. This previously uncharacterized function of CXCL12 was mediated by the atypical chemokine receptor ACKR3 (also known as CXCR7), required protein kinase A (PKA) activity, and induced chromatin compaction, which resulted in enhanced cell migration in 3D. Thus, we propose that chemical cues regulate the nuclear plasticity of migrating leukocytes to optimize their motility in restricted microenvironments.

INTRODUCTION

Neutrophils are key players in innate immune responses and provide potent defense against invading microbes. To reach sites of injury, circulating leukocytes have to cross the endothelial barrier and then navigate through interstitial spaces that are smaller than their own diameter (*1*). Therefore, the ability of leukocytes to rapidly readapt their shape in response to three-dimensional (3D) microenvironments is essential for immune responses, because increased cell rigidity results in their retention in capillaries and accumulation in postcapillary venules. The rheological properties and the topography of both the extracellular space and the cell itself control the maximal rate at which a cell can change its shape and transmigrate. Inside the cell, the cytoplasm facilitates cell migration because it contains the cytoskeletal elements required to deform the cell body and advance. Conversely, the volume of the nucleus inversely scales with the ability of a cell to migrate under confinement (*2*). Thus, the nucleus represents the main source of friction opposing cell locomotion in microenvironments with a high steric hindrance (*3*).

Several studies have described mechanical adaptation of the cell nucleus under 3D physical confinement by exploiting biophysical approaches, such as micropipette aspiration, atomic force microscopy, or substrate strain experiments with mesenchymal stem cells, cancer cell lines, and neutrophil-like HL-60 cells. The peculiar multilobular shape of the neutrophil nucleus is not essential for their rapid passage through micron-scale pores (*4*). So far, multiple studies have been performed to investigate the mechanisms of 3D neutrophil migration (*5*, *6*), and some of them reported the critical role of nuclear envelope composition in the migration of neutrophil-like HL-60 cells (*4*, *7*). However, the contribution of biochemical cues, such as chemokines, which regulate directed cell migration and positioning in organs, to the modulation of nuclear mechanical properties during cell migration remains unexplored.

In the organism, neutrophil homeostasis is maintained by a finely regulated balance between granulopoiesis, bone marrow storage and release, intravascular margination, clearance, and destruction. One of the main regulators of this process is the CXC chemokine CXCL12, which, by engaging its receptor CXCR4, participates in regulating neutrophil homeostasis (*8*), transendothelial migration (TEM) from the bone marrow to the bloodstream, and interstitial migration from the bloodstream toward inflamed peripheral tissues. CXCL12 inhibition prevents bone marrow neutrophil mobilization during polymicrobial sepsis, because CXCR4 and CXCL12 abundance is decreased within the bone marrow but increased in the peripheral tissues (*8*). However, the cellular mechanisms by which CXCL12 regulates neutrophil recirculation remain unclear. The aim of our work was to investigate the role of CXCL12 in the modulation of the biomechanical properties of the neutrophil nucleus and its effect on their migration through physically confined microenvironments.

[1]Department of Biomedical Sciences, University of Padova, Padova, Italy. [2]Fondazione Istituto di Ricerca Pediatrica Città della Speranza, Padova, Italy. [3]Institut Curie, PSL Research University, CNRS, UMR 144, F-75005 Paris, France. [4]Institut Pierre-Gilles de Gennes, PSL Research University, F-75005 Paris, France. [5]University of Verona, Department of Medicine, Division of General Pathology, Verona, Italy. [6]Venetian Institute of Molecular Medicine, Padova, Italy. [7]Department of Industrial Engineering, University of Padova, Padova, Italy. [8]Lymphocyte Cell Biology Unit, Department of Immunology, Institut Pasteur, INSERM-U1224, Ligue Nationale Contre le Cancer, Équipe Labellisée Ligue 2018, F-75015 Paris, France. [9]Sorbonne Université, Collège Doctoral, F-75005 Paris. France. [10]Université Paris Cité, INSERM UMR-S1151, CNRS UMR-S8253, Institut Necker Enfants Malades, F-75015 Paris, France.
*Corresponding author. Email: bianca.cali@ior.usi.ch (B.C.); pablo.vargas@inserm.fr (P.V.); antonella.viola@unipd.it (A.V.)
†Present address: Institute of Oncology Research, Oncology Institute of Southern Switzerland, CH-6500 Bellinzona, Switzerland.
‡These authors contributed equally to this work.

RESULTS

CXCL12 enhances nuclear adaptation of mouse neutrophils to confined environments

Because CXCL12 has a key role in regulating the maturation of neutrophils, their release from the bone marrow, and their retention at inflammatory sites (*9*), we first assessed the contribution of CXCL12 in modulating the migratory behavior of neutrophils. We purified primary neutrophils from the bone marrow of healthy wild-type mice and analyzed their motility in 3D collagen gels with customized, homemade polydimethylsiloxane (PDMS) chambers as previously described (*10*–*12*). Briefly, neutrophils were seeded in a high-density collagen gel (4 mg/ml; pore size: 1.173 ± 0.1507 μm; fig. S1A). While the cells were in the gel, they were incubated for 1 hour with CXCL12, which was then removed from the medium. Neutrophil motility in the collagen gels was then assessed for 4 hours by time-lapse video microscopy in the absence of any external chemokine gradient (movie S1). Under these conditions, neutrophils displayed random motility (Fig. 1A and fig. S1B). Detailed analysis of cell trajectories provided evidence that cells prestimulated with CXCL12 migrated over longer distances and were faster compared with unstimulated cells (Fig. 1, A to C). In addition, CXCL12-prestimulated neutrophils showed increased mean squared displacement (MSD), a parameter that indicates their enhanced capacity to move through their microenvironment (Fig. 1D). The increased motility stimulated by CXCL12 was sustained for at least 4 hours (fig. S1, B and C). Together, these data suggest that prestimulation with CXCL12 enhances neutrophil migration within dense collagen gels.

To further investigate the effect of CXCL12 on 3D neutrophil morphology, we exploited LifeAct-GFP (green fluorescent protein) bone marrow neutrophils (*13*) to visualize how these cells adapt their bodies to dense collagen matrices (fig. S1D). We allowed neutrophils to migrate in this 3D scaffold for 2 hours before they underwent fixation. We next imaged the samples by confocal microscopy and analyzed both the cell and nuclear sizes by 3D volume reconstruction (Fig. 1, E to G). Pretreatment with CXCL12 did not change cell size (Fig. 1G); however, the nuclei of the prestimulated neutrophils were ~40% smaller in comparison with those of control cells (Fig. 1G and movies S2 and S3).

To gain further insights into the cytoskeletal rearrangements stimulated by CXCL12 in restricted microenvironments, we analyzed LifeAct-GFP neutrophils migrating through custom microfabricated microchannels (3 μm wide by 4 μm high) (*10*, *12*). Within microchannels, cells move in only 1D, facilitating the analysis of cell trajectories, organelle positioning, and the organization of the cytoskeleton (*14*). Despite exhibiting increased migration speeds (fig. S1E), CXCL12-prestimulated cells did not show notable differences in actin organization compared with that in control cells. The enhanced migration speed stimulated by CXCL12 was not associated with an obvious accumulation of actin filaments either around or behind the nuclei (fig. S1, F and G) as was previously shown (*15*). However, the nuclei in CXCL12-stimulated neutrophils showed lower aspect ratios and higher circularity compared with those of control cells (fig. S1, H and I). These findings suggest that CXCL12 prestimulation results in increased neutrophil migration, which does not relate to substantial changes in cell size or actin cytoskeletal organization but is associated with increased nuclear deformation.

To further investigate the consequences of CXCL12-induced nuclear deformation on cell motility, we took advantage of customized microfabricated devices to analyze neutrophil migration through highly constrained microenvironments. For this purpose, we used straight microchannels (8 μm wide by 4 μm high) coupled to 1-μm side constrictions (Fig. 1, H and I, and movie S4) (*15*). In this system, cells deform and squeeze their nuclei to efficiently migrate through micrometer-size holes. Our results showed that CXCL12-prestimulated neutrophils were ~34% faster than control cells in crossing the constrictions (Fig. 1, H and I), suggesting that CXCL12-induced nuclear pliability could facilitate neutrophil migration through highly restricted microenvironments.

On the basis of these results, we focused on alternative methodologies to measure the mechanical properties of neutrophil nuclei. One of these methods involved micropillars, 3D-patterned structures that may influence the rheological properties of the nuclei of cancer cells, inducing their deformation (*16*). Taking advantage of these tools, we evaluated nuclear deformability upon exposure to CXCL12 (Fig. 1, J and K) (*17*). We seeded primary mouse neutrophils that were prestimulated with or without CXCL12 on top of fibronectin-coated micropillars. After 30 min, the cells were fixed and analyzed by confocal microscopy to visualize the extent of nuclear deformation between the micropillars. We observed that the nuclei of control neutrophils were mostly donut shaped and primarily restrained to the tops of the pillars (Fig. 1, J and K, and movie S5). In contrast, CXCL12-prestimulated neutrophils showed more deformed nuclei that inserted between the pillars, mostly accumulating at the bottom of the 3D pattern (Fig. 1, J and K, and movie S5). The increased distribution of the nuclear volume at the bottom of the micropillars suggests that CXCL12 fosters the deformability of the cell nuclei (Fig. 1K). Therefore, we hereafter considered the percentage of nuclear content embedded at the bottom of the patterned substrate to be an index of nuclear deformability (*16*). We also observed the same induction of nuclear deformability in human blood granulocytes exposed to CXCL12 (fig. S2, A to C). This result indicates that CXCL12 also increased nuclear deformability in human samples. Together, these findings provide evidence that chemotactic signals contribute to the regulation of the nuclear plasticity needed to facilitate cell movement under strong physical constraints.

CXCL12 enhances nuclear deformability by engaging ACKR3

CXCL12 was initially described to bind to the receptor CXCR4; however, CXCL12 also binds to the atypical chemokine receptor 3 (ACKR3) (also known as CXCR7) (*18*). Dimeric CXCL12 also binds to ACKR1 in Madin-Darby canine kidney cells and erythrocytes (*19*). CXCL12 is constitutively expressed by many endothelial cell types and promotes the arrest and TEM of leukocytes under physiological shear flow by binding to CXCR4. Note that although ACKR3 does not stimulate chemotactic responses, its scavenging activity generates guidance cues for the directional migration of CXCR4-expressing human endothelial cells and supports CXCR4-mediated integrin activation in response to CXCL12 (*20*).

To characterize the signals stimulated by CXCL12 that modulate the mechanical response of neutrophil nuclei, we first verified the contribution of CXCR4 to the regulation of nuclear deformability. Thus, we measured nuclear deformation in micropillars in the presence of either AMD3100, a small-molecule inhibitor of CXCL12

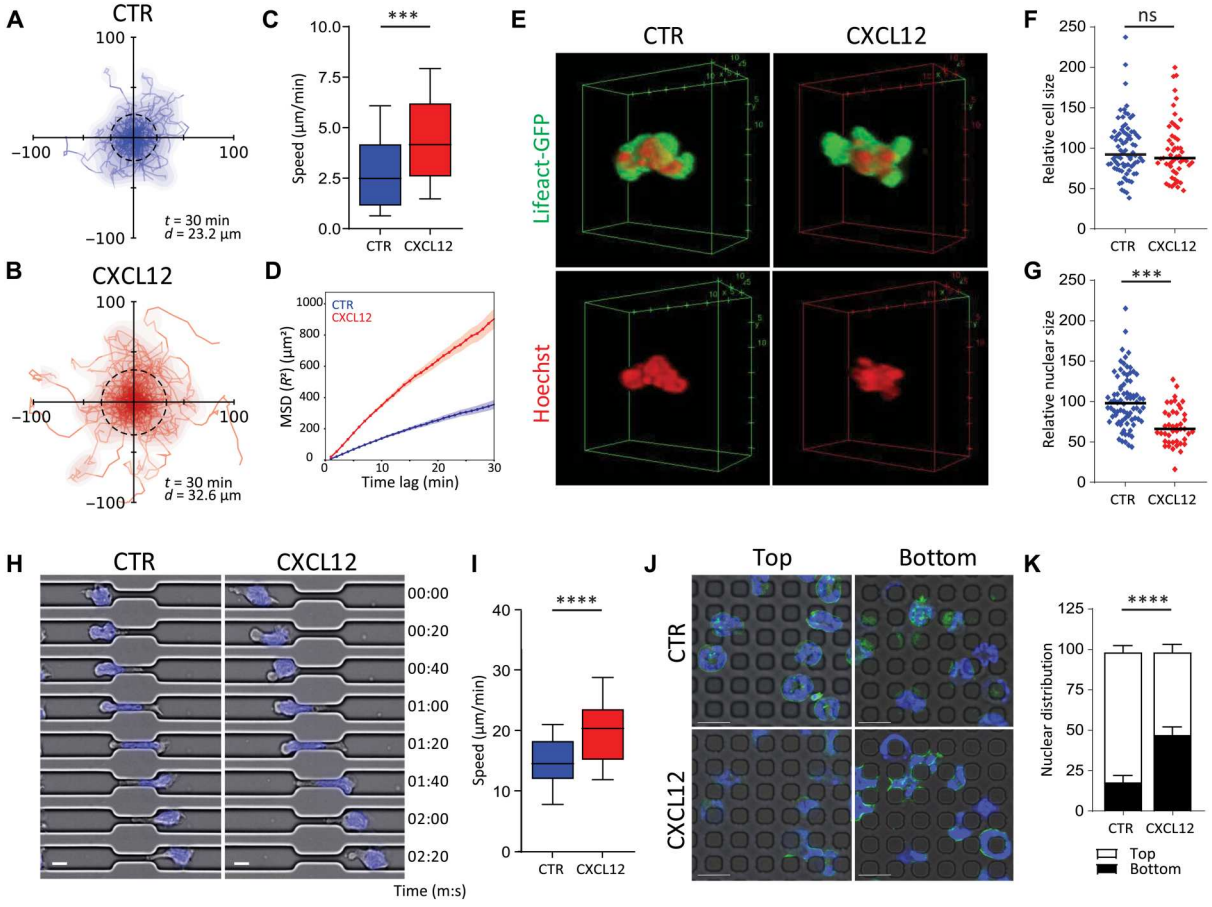

Fig. 1. CXCL12 enhances the nuclear adaptation of neutrophils to confining microenvironments. (**A** and **B**) Representative trajectories of control (CTR) (A) versus CXCL12-prestimulated (B) neutrophils migrating through dense rat tail collagen gels (4 mg/ml). *t* indicates the duration of the trajectories, and *d* is the average displacement of each dataset. (**C** and **D**) Speed (C) and mean squared displacement (MSD) (D) of the cell trajectories shown in (A) and (B). Data are representative of three independent experiments. In (C), ***$P < 0.001$ by Mann-Whitney test. (**E**) 3D rendering of LifeAct-GFP (green) mouse neutrophils migrating in collagen gels. Cells were labeled with Hoechst (red) and imaged as migrating in the 3D gels. (**F** and **G**) Relative cell sizes (F) and nuclear sizes (G) of mouse neutrophils as shown in (E); $n = 80$ cells for the CTR and $n = 53$ cells for the CXCL12 pretreatment. Data are representative of three independent experiments. ***$P < 0.001$ by Mann-Whitney test. ns, not significant. (**H**) Representative images of Hoechst-labeled mouse neutrophils (blue) migrating through a microconstriction (length = 15 µm; width = 1 µm). Time is given as minutes:seconds. Scale bars, 5 µm. (**I**) Quantification of the speed of passage of mouse neutrophils through microconstrictions as shown in (H); $n = 58$ cells for the CTR and $n = 100$ cells for CXCL12). Data are representative of three independent experiments. ****$P < 0.0001$ by Mann-Whitney test. (**J**) Representative confocal images of control (CTR) or CXCL12-prestimulated mouse neutrophils seeded on micropillars. Cells were fixed and stained for F-actin (green). Nuclei were counterstained with Hoechst (blue). Top: neutrophils that were retained on the pillar apex. Bottom: cells that moved down to the substrate base and inserted between the micropillars. Scale bars, 10 µm. (**K**) Percentage of nuclear distribution along the vertical axis of micropillars as shown in (J). Data are means ± SEM of three independent experiments. ****$P < 0.0001$ by Mann-Whitney test.

signaling that prevents chemokine binding to its canonical receptor CXCR4, or pertussis toxin (PTx), a specific inactivator of $G\alpha_i$, the G protein coupled to CXCR4 involved in chemotaxis. Neither AMD3100 nor PTx significantly inhibited CXCL12-induced nuclear deformability, suggesting that a CXCR4-independent signaling pathway was responsible for this function (Fig. 2, A and B).

ACKR3 expression in mouse leukocytes is still controversial. Although it is thought that mouse and human leukocytes do not express ACKR3 (*20*), several studies provided evidence that ACKR3 is involved in T cell adhesion (*21*), B cell retention in the marginal zone of the spleen (*22*), and granulocyte accumulation in the lungs in a mouse model of acute pulmonary inflammation (*23*). Note that ACKR3 is involved in the TEM of neutrophils in mouse models of lung inflammation and in the TEM of cancer cells, two processes for which nuclear deformation is critical (*23*). We thus verified the expression of CXCL12 receptors in mouse bone marrow neutrophils by real-time polymerase chain reaction (PCR) analysis, and we detected the presence of both *Cxcr4* and *Ackr3* mRNAs (fig. S3, A to C). In addition, the amounts of both *Cxcr4* and *Ackr3* mRNAs were maintained when the cells were kept in culture for a few hours (fig. S3, B and C). Furthermore, we verified cell surface ACKR3 expression by flow cytometry, and we observed that, although only a very small fraction of neutrophils expressed CXCR7 on their cell surface, 99% of the neutrophils had detectable intracellular CXCR7 (fig. S3, D and E). These data were also confirmed by immunogold labeling and electron microscopy analysis of neutrophils isolated from mouse bone marrow (fig. S3F).

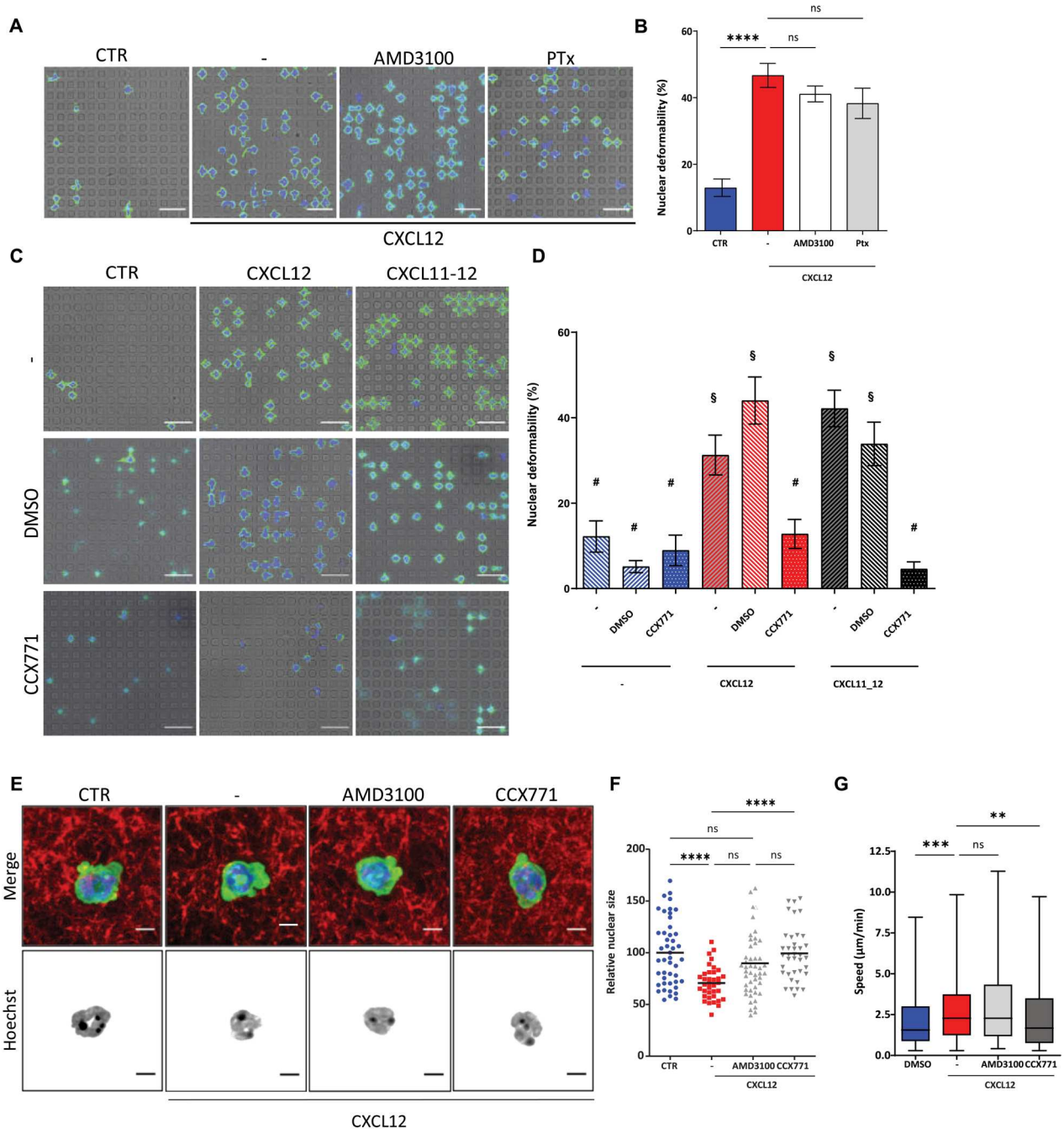

Fig. 2. ACKR3 engagement modulates nuclear adaptation of mouse neutrophils. (**A**) Representative confocal images of mouse neutrophils gathered at the bottom of micropillars under control or CXCL12-prestimulated conditions. Where indicated, cells were preincubated with AMD3100 or pertussis toxin (Ptx). The actin cytoskeleton was stained with Phalloidin-Alexa488 (green), and nuclei were counterstained with Hoechst (blue). Scale bars, 20 µm. (**B**) Quantification of nuclear deformability (%) from the experiments shown in (A). At least four stacks per condition were analyzed from three independent experiments. ****$P < 0.0001$ by Kruskal-Wallis test with Dunn's correction for multiple comparisons. (**C**) Representative confocal images of neutrophils stimulated with CXCL12 or CXCL11_12 that had gathered at the bottom of micropillars. Where indicated, cells were preincubated with CCX771 before being stimulated with chemokine. Scale bars, 20 µm. (**D**) Quantification of nuclear deformability (%) from the experiments shown in (C). Dimethyl sulfoxide (DMSO) was used as a vehicle control for CCX771. At least four image stacks per condition were analyzed from three independent experiments. Bars with different symbols are statistically different from each other. $P < 0.05$ by Kruskal-Wallis test with Dunn's correction for multiple comparisons. (**E**) Maximal projection of confocal images showing neutrophil shape (LifeAct-GFP, green) migrating into TAMRA-labeled 3D rat tail collagen gels (red). Neutrophils were preincubated with AMD3100 or CCX771 before stimulation with CXCL12. Scale bars, 10 µm. (**F**) Analysis of the relative nuclear size of CXCL12-stimulated neutrophils in collagen matrix (4 mg/ml) in the presence of AMD3100 or CCX771 ($n = 46$ cells for CTR, $n = 36$ cells for CXCL12, $n = 46$ cells for CXCL12 + AMD3100, and $n = 38$ cells for CXCL12 + CCX771). Data are representative of three independent experiments. ****$P < 0.0001$ by Kruskal-Wallis test with Dunn's correction for multiple comparisons. (**G**) Average speed of CXCL12-prestimulated neutrophils that migrated through collagen gels in the presence of AMD3100 or CCX771. Data are representative of three independent experiments. **$P < 0.01$ and ***$P < 0.001$ by Kruskal-Wallis test with Dunn's correction for multiple comparisons.

Therefore, we evaluated the involvement of ACKR3 in the induction of nuclear deformation in bone marrow neutrophils. We assessed chemokine-induced nuclear deformability in the presence of CCX771, a small molecule that binds with high affinity and selectivity to ACKR3, inhibiting the TEM of cancer cells (*24*). Note that ACKR3 inhibition by CCX771 prevented nuclear deformation and accumulation at the bottom of the micropillars upon exposure to CXCL12 (Fig. 2, C and D). The role of ACKR3 in neutrophil nuclear deformation was further confirmed in experiments with CXCL11_12, an engineered, chimeric, chemokine-like ligand that selectively binds with high affinity to ACKR3 (Fig. 2, C and D) (*25*). In addition, we observed that the chemokine CXCL11, a natural ACKR3 ligand, also enhanced the nuclear deformability of neutrophils on micropillars (fig. S3, G and H). Furthermore, stimulation of neutrophils with CXCL11_12 increased their speed when migrating in 3D collagen gels (fig. S3I).

We then assessed the contributions of signaling by CXCR4 and ACKR3 to CXCL12-induced nuclear adaptation and 3D migration in dense collagen matrices. Exploiting this system, we observed that ACKR3 inhibition hindered the nuclear size decrease induced by CXCL12 (Fig. 2, E and F). Conversely, CXCR4 antagonism had no significant effect on CXCL12-induced nuclear adaptation to confined microenvironments (Fig. 2, E and F). Consistent with these observations, we observed that CXCR4 antagonism had no effect on random neutrophil motility through collagen gels, whereas ACKR3 inhibition significantly inhibited the CXCL12-enhanced 3D migration of neutrophils (Fig. 2G). Together, these findings provide evidence of a role for ACKR3 signaling in the induction of nuclear deformation and 3D migration of mouse neutrophils.

The CXCL12-ACKR3 axis stimulates PKA activity

ACKR3 does not stimulate G protein–dependent signaling and lacks the conserved DRYLAIV motif necessary for coupling to $G\alpha_i$ proteins, which inhibit adenylyl cyclase activity and thus reduce cyclic adenosine 3′,5′-monophosphate (cAMP) production. ACKR3 has long been considered a "decoy receptor," because it fails to mobilize Ca^{2+} from intracellular or extracellular sources after ligand engagement. However, ACKR3 may form functional heterodimers with CXCR4, thus interfering with CXCR4-induced $G\alpha_i$ activation (*26*). Because CXCL12 induced nuclear deformability on micropillars when $G\alpha_i$ proteins were inhibited (Fig. 2, A and B), we assessed cAMP production in bone marrow mouse neutrophils upon ACKR3 engagement. We detected a significant increase in cytosolic cAMP concentration when cells were stimulated with CXCL12 in the presence of the CXCR4 antagonist AMD3100 (Fig. 3B). Hence, we speculate that the increase in cAMP concentration associated with the CXCL12-ACKR3 axis might enhance neutrophil nuclear deformability. To verify this hypothesis, we stimulated neutrophils with forskolin, which directly activates adenylyl cyclases and thus cAMP production. Using micropillars, we found that a forskolin-induced increase in intracellular cAMP concentration (Fig. 3B) was sufficient to trigger nuclear deformability in neutrophils (Fig. 3, C and D). Functionally, this treatment was sufficient to increase neutrophil migration in 3D collagen gels (Fig. 3E).

The second messenger cAMP mediates its biological effects primarily through its activation of cAMP-dependent protein kinase (PKA). To investigate whether CXCL12-ACKR3 signaling enhanced nuclear deformability through PKA activation, we preincubated cells with the myristoylated PKA inhibitor (14-22) amide (myr-PKI) before stimulating them with CXCL12. Image analysis of cells on micropillars showed that CXCL12 required PKA activity to enhance nuclear deformability because most of the nuclei did not adapt to the topography of the substrate and were retained at the top of the patterned structure (Fig. 3, F and G). Similarly, PKA inhibition also reduced CXCL12-enhanced neutrophil migration in collagen gels (Fig. 3H). Consistent with this finding, PKA inhibition also affected nuclear adaptation to a high-density 3D collagen matrix (fig. S4, A and B). Together, these data suggest that CXCL12 modulates neutrophil nuclear deformability through a cAMP-PKA pathway activated by ACKR3 engagement.

The ACKR3-PKA axis facilitates TEM by neutrophils

Although CXCL12 is primarily involved in the regulation of neutrophil mobilization and homeostasis, several reports indicate that CXCL12 supports neutrophil recruitment to peripheral inflamed tissues in mouse models of acute lung injury, polymicrobial sepsis, and peritonitis (*8*). Several studies already reported that ACKR3 engagement does not stimulate chemotaxis but that its scavenging activity supports directional migration and integrin activation in CXCR4-expressing cells in response to CXCL12 (*21*). On the basis of our results showing a pivotal role of the ACKR3-PKA axis in the induction of chemokine-induced nuclear adaptation and 3D migration, we hypothesized that ACKR3 might have a role in promoting TEM, which requires leukocyte nuclear deformation, in response to chemoattractants. We first verified the effect of inhibiting CXCR4, ACKR3, and PKA on neutrophil chemotaxis toward CXCL12 using the 3-μm-pore-size transwell assay (fig. S5, A to D). As expected, CXCR4 inhibition prevented the chemotaxis of mouse neutrophils toward CXCL12 (fig. S5B), whereas ACKR3 blockage did not affect the directional migration of these cells (fig. S5C). In addition, and consistent with other studies (*27*), we observed that PKA activity was not required for directional migration of neutrophils toward CXCL12, as shown by the fact that PKA inhibition significantly increased chemotaxis (fig. S5D).

We then analyzed the effect of inhibiting CXCR4, ACKR3, and PKA on the TEM of neutrophils toward the bacterial peptide and chemoattractant *N*-formyl-met-leu-phe (fMLP; Fig. 4, A to C). TEM assays were performed by coating the upper surface of the transwell inserts with a monolayer of SVEC4-10 mouse endothelial cells. Under these experimental conditions, neutrophils have to squeeze through the endothelial barrier, which constitutively expresses CXCL12, to reach the lower chamber of the transwells containing the fMLP. Although neither CXCR4 nor ACKR3 is required for directional migration toward fMLP, the use of either AMD3100 or CCX771 resulted in decreased neutrophil migration through the endothelium (Fig. 4, A to C). Furthermore, we observed that PKA inhibition significantly reduced the number of transmigrating neutrophils toward fMLP (Fig. 4C). Note that myr-PKI did not affect directional migration toward fMLP (fig. S6A). Because efficient TEM requires the fine-tuning of integrin-mediated leukocyte adhesion to the endothelium (*1*), we also examined neutrophil adhesion to immobilized intercellular adhesion molecule–1 (ICAM-1). We observed that inhibition of CXCR4, which stimulates integrin activation (*21*), reduced neutrophil adhesion to immobilized ICAM-1 (fig. S6B). However, inhibition of ACKR3 did not impede

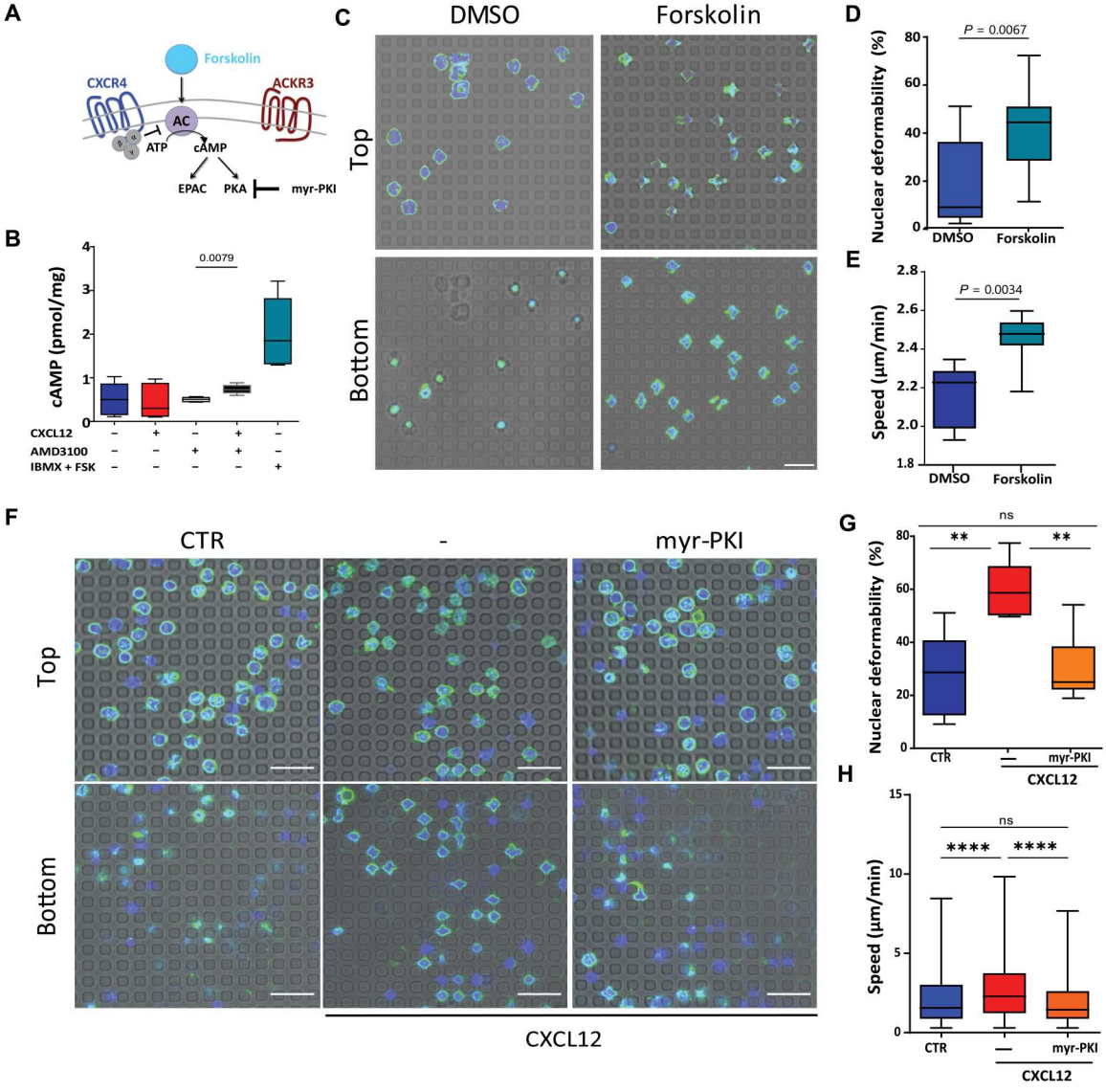

Fig. 3. cAMP-PKA activity is critical for neutrophil nuclear adaptation and 3D migration. (**A**) Schematic representation of CXCL12 receptor signaling linked to cAMP signals. Gα proteins modulate AC activities. Activation is shown by the arrows, and inhibition is shown by the blunt arrows. (**B**) Intracellular cAMP concentration in cells treated under the indicated conditions was determined by ELISA. The phosphodiesterase (PDE) inhibitor IBMX and the AC activator forskolin were used as internal positive controls. The cAMP concentration was normalized to the amount of protein in the cell lysates (picomoles per milligram). Data are pooled from five independent experiments and were analyzed by Mann-Whitney test. (**C** and **D**) Representative images (C) and quantification of nuclear deformability (D) in forskolin-treated neutrophils and DMSO-treated control cells. Scale bar, 20 μm. Statistical significance was determined by the Mann-Whitney test. (**E**) Average speed of neutrophils randomly migrating through collagen gels in the presence of forskolin. DMSO was used as a control. Plot shows medians from duplicate samples from three independent experiments. Significance was determined by the Mann-Whitney test. (**F**) Representative confocal images of the nuclear distribution of CXCL12-prestimulated mouse neutrophils along the vertical axis of micropillars in the presence or absence of the PKA inhibitor myr-PKI. Top: Cells retained at the apex of the patterned substrates. Bottom: Cells with deformed nuclei accumulated at the bottom. Scale bars, 20 μm. (**G**) Quantification of nuclear deformability (%) from the experiments shown in (F). $^{**}P < 0.01$ by Kruskal-Wallis test with Dunn's correction for multiple comparisons. (**H**) Speed of neutrophils that were prestimulated with CXCL12 in the presence or absence of myr-PKI and then randomly migrated through collagen gels. $^{****}P < 0.0001$ by Kruskal-Wallis test with Dunn's correction for multiple comparisons.

neutrophil adhesion to ICAM-1 but, in contrast, resulted in a slight increase in the number of attached cells (fig. S6C).

Next, on the basis of our earlier results showing that ACKR3 modulates nuclear deformation in restricted microenvironments, we took advantage of microfabricated constrictions to evaluate the contribution of each CXCL12 receptor to the passage of neutrophils through 1-μm side gaps. As expected, CXCL12-treated neutrophils migrated more efficiently than did control cells through the small holes (Fig. 4D). Although inhibition of CXCR4 had no effect on neutrophil passage through the 1-μm constrictions, ACKR3 and PKA signaling were both required to enhance the passage of these cells through the narrow gaps (Fig. 4D). Together, these results indicate that CXCR4 and ACKR3 receptors play distinct and nonredundant roles during neutrophil migration.

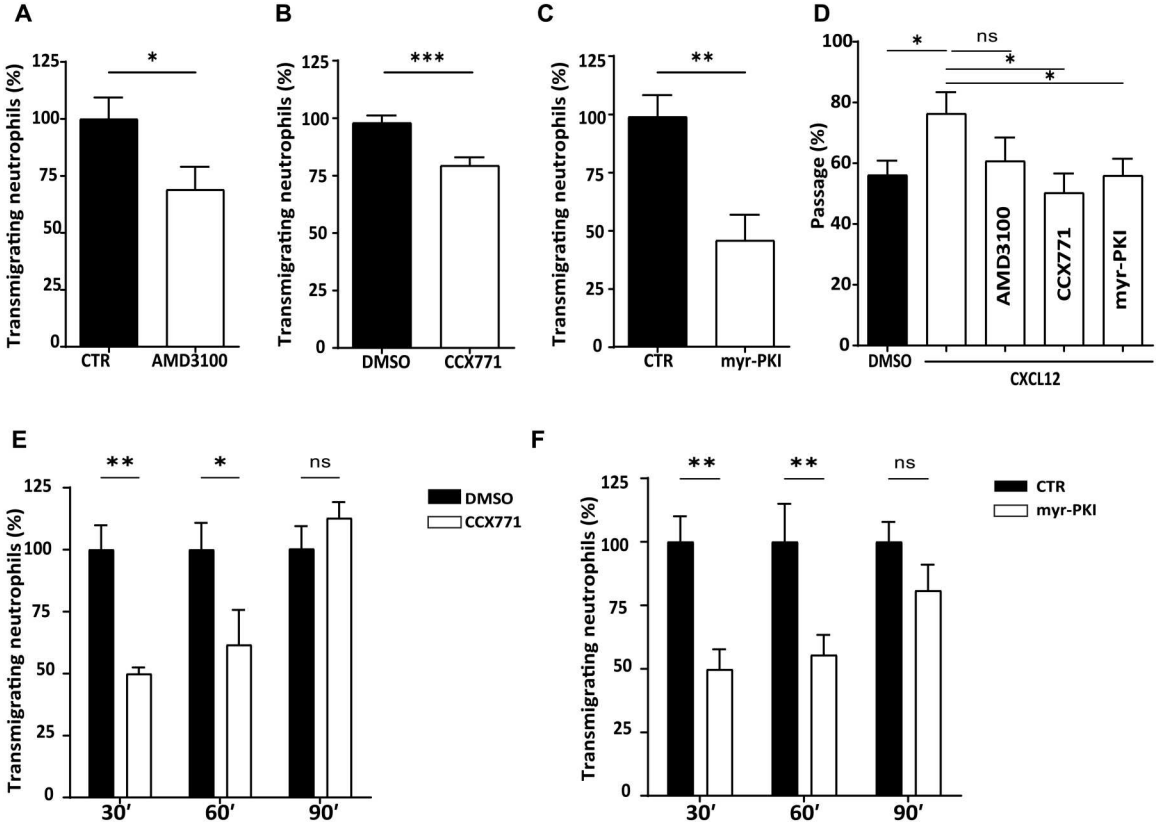

Fig. 4. The ACKR3-PKA axis modulates nuclear squeezing to support neutrophil TEM. (**A** to **C**) Neutrophil TEM toward fMLP was assessed with 3.0-μm transwell inserts coated with a layer of tumor necrosis factor–α (TNF-α)–activated SVECs. (A) TEM of neutrophils preincubated with AMD3100 was analyzed by counting the number of cells in the lower chamber after 1 hour of migration. Data are means ± SD of three independent experiments and were analyzed by Mann-Whitney test. (B) TEM of neutrophils toward fMLP after preincubation with CCX771. DMSO was used as a control (set at 100%). Data are means ± SD of four independent experiments and were analyzed by Mann-Whitney test. (C) TEM toward fMLP of neutrophils preincubated with myr-PKI. Data are means ± SD of three independent experiments and were analyzed by Mann-Whitney test. (**D**) Efficiency of neutrophil passage through 1-μm side constrictions is expressed as the percentage of cells that passed the constriction relative to the total number of neutrophils that encountered it. Data are means ± SD of two fields of view from three independent experiments (n = 225 cells for DMSO; n = 201 for CXCL12; n = 178 for AMD3100; n = 146 for CCX771; and n = 186 for myr-PKI) and were analyzed by Mann-Whitney test. (**E** and **F**) Neutrophil TEM toward fMLP was analyzed after 30, 60, and 90 min of migration. TEM toward fMLP of neutrophils preincubated with CCX771 (E) or myr-PKI (F) was analyzed at the indicated times. Cell numbers were normalized relative to DMSO-treated control cells (E) or untreated cells (F), which were set at 100%. Data are means ± SD of three independent experiments and were analyzed by two-way analysis of variance (ANOVA), followed by Sidak's multiple comparisons test (**P < 0.01 and *P < 0.05).

Whereas CXCR4 signaling is required for neutrophil chemotaxis and integrin adhesion, the ACKR3-PKA axis is a key determinant of 3D cellular migration by inducing nuclear deformability. Therefore, we hypothesized that the ACKR3-PKA axis might increase the efficiency of neutrophil TEM by influencing its kinetics. Thus, we analyzed TEM kinetics (at 30, 60, and 90 min) in the presence of either CCX771 (Fig. 4E) or myr-PKI (Fig. 4F). We found that inhibition of either ACKR3 (Fig. 4E) or PKA (Fig. 4F) hindered neutrophil TEM at early times but had no significant effect when samples were analyzed after 90 min of TEM. Together, these results provide evidence that ACKR3-PKA signals play a crucial role in modulating neutrophil nuclear shape and thus facilitate the efficient TEM of these cells.

The ACKR3-PKA axis promotes chromatin compaction

The mechano-physical properties of cell nuclei are dependent on two main structural determinants: the composition of the nuclear envelope and the chromatin organization. The nuclear lamina consists of two major forms of intermediate filaments: A-type lamins (lamin A and C) and B-type lamins (lamin B1 and B2). Increased amounts of lamin A markedly influence the ability of neutrophil-like HL-60 cells to pass through micrometer-scale constrictions (*4*) and prevent their motility through collagen I matrices without affecting TEM (*7*). However, in comparison with those of HL-60 cells, the nuclear envelopes of human blood neutrophils contain low-to-negligible amounts of several nuclear envelope proteins, including lamin A/C (*28*). Therefore, we first analyzed lamin A abundance in neutrophils purified from mouse bone marrow. As expected, we did not detect any signal by Western blotting analysis in which we used bone marrow–derived dendritic cells as a positive control (fig. S7A). Thus, we excluded a key role for lamin A regulation in chemokine-enhanced nuclear deformability in neutrophils.

Accumulating evidence has shown that chromatin condensation also contributes to nuclear mechanics and cell migration, because increased euchromatin or decreased heterochromatin softens

nuclei (*29*). Thus, we hypothesized that chemokine exposure might change the structural chromatin status of mouse neutrophils. Heterochromatin markers commonly found at the nuclear periphery include H3K9me1, H3K9me2, H3K9me3, H3K56me3, H4K20me2, H4K20me3, H3K27me2, H3K27me3, and H3K4ac. Both mouse and human blood neutrophils under basal conditions exhibit high abundance of H3K9me2, H3K27me1, H3K27me2, and H3K27me3, whereas H4K20me2 is relatively less abundant (*30*). Because H4K20 dimethylation is catalyzed by Suv420H1 and Suv420H1 is one of the most abundant histone methyltransferases in bone marrow neutrophils (fig. S7B) (*31*), we hypothesized that chemokine signals might promote nuclear reshaping by affecting H4K20 dimethylation. To address this hypothesis, we assessed Suv420H1 abundance in mouse bone marrow neutrophils by Western blotting analysis (fig. S7C) and then used immunofluorescence to assess the relative amounts of H4K20me2 in neutrophils exposed to stimuli that induced nuclear deformation (Fig. 5, A to C). We found that upon stimulation with CXCL12, CXCL11_12, or forskolin, neutrophil nuclei showed higher positivity for H4K20me2 compared with those of unstimulated, control cells (Fig. 5, A and B). Furthermore, under these conditions, the nuclear area was significantly reduced (Fig. 5C). These data suggest that the signaling modulating nuclear plasticity in neutrophils is associated with the regulation of the heterochromatin abundance.

Thus, to verify the contribution of chromatin compaction to neutrophil 3D migration, we analyzed neutrophil motility in collagen gels in the presence of the Suv420H1 inhibitor, A-196 (*32*). We observed that the inhibition of H4K20 dimethylation reduced neutrophil motility in 3D collagen gels (Fig. 5D). Furthermore, when Suv420H1 was inhibited, stimulation of neutrophils with either CXCL12 or CXCL11_12 failed to increase their migratory speed through the collagen gels (Fig. 5D). In addition, by analyzing neutrophil TEM toward fMLP in the presence of A-196, we observed a significant reduction in the percentage of transmigrating neutrophils (Fig. 5E). These data suggest that histone modifications regulate neutrophil motility in a 3D microenvironment, because H4K20 methylation is sufficient to enhance their migration within interstitial spaces and through the endothelial cell barrier. Together, our data indicate that CXCL12 signaling through ACKR3 promotes neutrophil migration through challenging microenvironments by inducing chromatin condensation upon H4K20 dimethylation. These results suggest a role for chemoattractants in the regulation

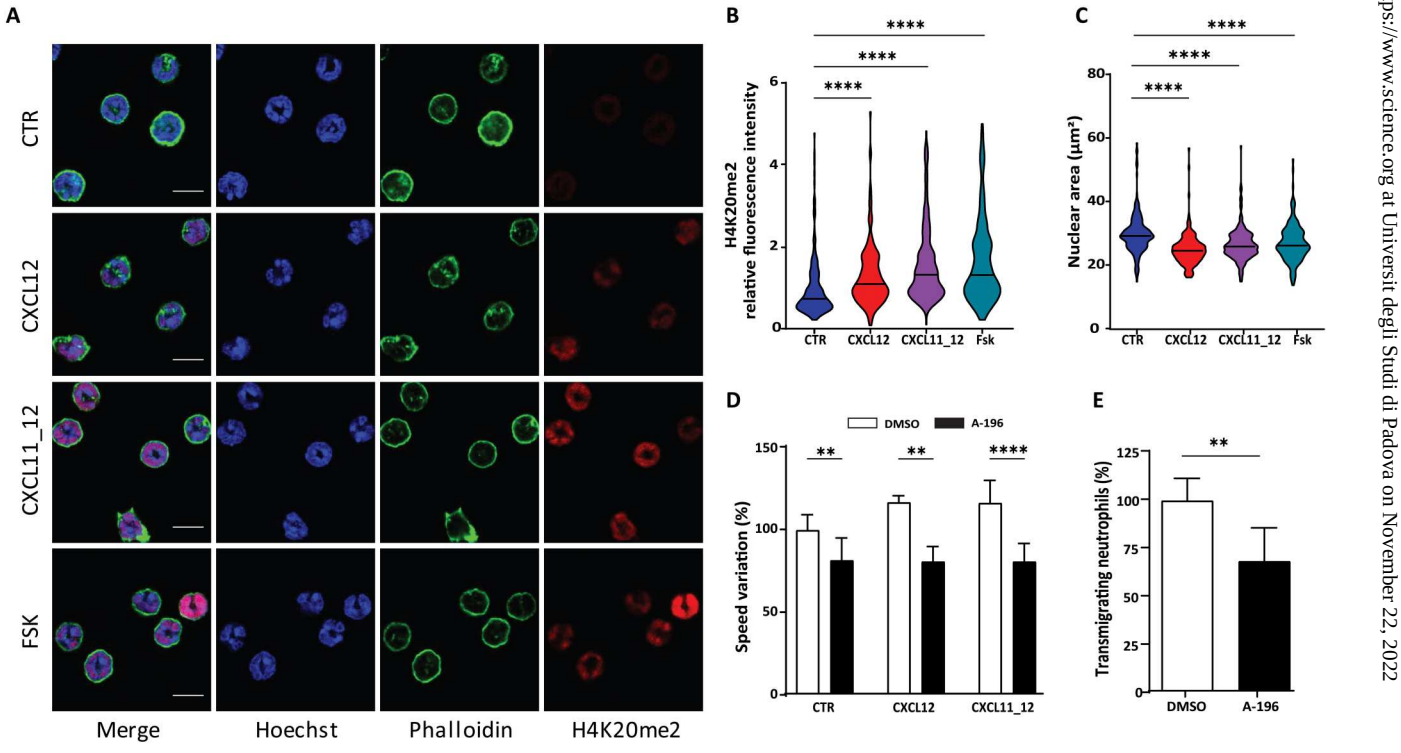

Fig. 5. Chemokine signals promote chromatin compaction. (**A**) Representative confocal images of mouse neutrophils stimulated with CXCL12, CXCL11_12, or forskolin (FSK) for 30 min before fixation and immunostaining with anti-H4K20me2 antibody (red). Cells were stained for the actin cytoskeleton with phalloidin (green), whereas Hoechst (blue) was used for nuclear counterstaining. Scale bars, 7 µm. (**B** and **C**) Quantification of the fluorescence intensity of H4K20me2 heterochromatin marker (B) and the measured nuclear areas (C) of neutrophils stimulated with CXCL12, CXCL11_12, or Forskolin. Data in (B) were normalized relative to the median of the untreated control cells (n = 213 cells for CTR; n = 170 for CXCL12; n = 243 for CXCL11_12; n = 197 for FSK). ****$P < 0.0001$ by Kruskal-Wallis test with Dunn's correction for multiple comparisons. (**D**) Analysis of the effect of Suv420H1 inhibition on the speed of neutrophils prestimulated with CXCL12 or CXCL11_12 and then allowed to randomly migrate through collagen gels. Data are means ± SD of duplicate samples from three independent experiments and were analyzed by Kruskal-Wallis test with Dunn's correction for multiple comparisons; **$P < 0.01$ and ***$P < 0.001$. (**E**) TEM of neutrophils preincubated with A-196 was analyzed by counting the number of cells in the lower chamber after 1 hour of migration. DMSO was used as a control (set at 100%). Data are means ± SD of two independent experiments and were analyzed by Mann-Whitney test (**$P < 0.01$).

of nuclear morphology for the optimization of cell migration in dense microenvironments.

DISCUSSION

The squeezing of cells through narrow spaces is a critical requirement for the immune response and metastasis. In this process, the position and dynamics of the cell nucleus strongly affect cell migration. Thus, alterations in nuclear structure and composition are usually associated with human diseases, such as muscular dystrophy, dilated cardiomyopathy, premature aging, and cancer. For neutrophils, their continuous trafficking through the body depends on their passage through endothelial barriers as well as their migration in tissues, both of which are associated with nuclear squeezing through narrow openings. The CXCL12-CXCR4 axis is a master regulator of neutrophil retention and mobilization in the bone marrow as well as of neutrophil clearance during inflammatory responses. Although CXCL12 is a weak chemoattractant for isolated murine blood neutrophils in comparison with the highly responsive Jurkat cells, studies of human neutrophils showed that these cells respond robustly to CXCL12 even when they express very low amounts of CXCR4 (*33*). Furthermore, senescent, $CXCR4^{hi}$ mouse neutrophils are cleared from the blood when CXCL12 amounts are maximal in the bone marrow (*34*).

Here, we demonstrated that the stimulation of neutrophils with CXCL12 promoted their migration through tiny pores by enhancing their nuclear deformability. This finding suggests that CXCL12 signaling may influence neutrophil egress from the bone marrow or their TEM at peripheral tissues by altering the physical properties of their nuclei. Our work provides evidence that chemokines can determine the mechanical adaptation of the nuclei to constraining 3D environments. Mechanistically, most studies investigating 3D neutrophil migration provided evidence of a key role for actomyosin contraction and microtubule polymerization in supporting cell transmigration and migration in collagen gels (*5*, *6*). We previously showed that in dendritic cells, Arp2/3-driven actin polymerization around the nucleus disrupts the nuclear lamina to enable nuclear deformation and facilitate cell migration through narrow pores (*15*). Note that we did not observe any substantial enrichment of actin around the nucleus in CXCL12-stimulated neutrophils. This might be due to the absence of lamin A/C in bone marrow neutrophils, which makes Arp2/3 unnecessary for their deformation. These findings are consistent with our previous observations that showed that Arp2/3-dependent perinuclear actin nucleation was dispensable for the passage of dendritic cells through small constrictions when lamin A/C was depleted (*15*).

Furthermore, we found that CXCL12 regulated neutrophil migration by activating two different signaling pathways downstream of two different receptors that play nonredundant roles in cell migration: CXCR4 and ACKR3. The expression of ACKR3 in mouse and human neutrophils is controversial (*20*). However, several studies have provided evidence that ACKR3 is involved in granulocyte accumulation in the lungs in a mouse model of acute pulmonary inflammation (*23*). To our knowledge, ACKR3 KO mouse models are still lacking. Homozygous animals die during the perinatal period and have ventricular septal defects and semilunar valve malformations. Therefore, we used CXCL11_12 chimera (*25*) and CCX771 (*35*) as tools to specifically study ACKR3 function in mouse neutrophils, and we showed that ACKR3 plays a critical role in sustaining CXCL12-induced nuclear deformation and 3D cellular migration. Our data thus suggest that the signaling pathways downstream of CXCR4 and ACKR3 ultimately combine to coordinate cell motility, cell adhesion, and nuclear pliability to sustain migration in 3D. Whereas CXCR4 was necessary for chemotaxis and integrin-mediated cell adhesion, the enhancement of nuclear deformation required CXCL12 binding to its atypical receptor ACKR3. Despite the fact that ACKR3 has been long considered a silent receptor, it stimulates specific cell functions that primarily control cell migration (*24*, *26*). Signaling downstream of ACKR3 engagement has not been fully elucidated, and it has been mainly ascribed to β-arrestin recruitment (*36*). Our data indicate that CXCR4 and ACKR3 signaling coexist in mouse bone marrow neutrophils and modulate cAMP abundance. Whereas CXCR4 signaling was necessary for chemotaxis and integrin-mediated adhesion, the ACKR3 pathway enhanced nuclear deformation upon CXCL12 binding.

We previously demonstrated that the heterodimerization of CXCR4 and CCR5 activates signaling by G_q and/or G11 or both instead of the conventional G_i pathway (*37*, *38*). Furthermore, ACKR3 can heterodimerize with CXCR4, modulating G protein signaling in Chinese hamster ovary cells (*26*). Therefore, ACKR3 might modulate CXCR4 signaling and eventually lead to an increase in cAMP concentration. In this scenario, the presence of AMD3100 might affect the binding of CXCL12 to ACKR3 (*39*). It has also been demonstrated by proximity ligation assays and coimmunoprecipitation experiments that ACKR3 forms heteromeric complexes with $\alpha_{1A/B/D}$-adrenergic receptors (ARs) in vascular smooth muscle cells (*40*, *41*). ARs couple to phosphoinositide hydrolysis, adenylyl cyclase, and mitogen-activated protein kinase pathways (*42*). ARs are present on immune cells, including neutrophils (*43*). Hence, we speculate that CXCL12 binding to ACKR3 might stimulate the activation of G_q proteins coupled to the α_{1A}AR, eventually leading to the protein kinase C–dependent stimulation of cAMP generation (*44*). Here, we showed that ACKR3 engagement was associated with an increase in cytosolic cAMP concentration. However, whether adenylyl cyclases are directly activated through G_s proteins or as a consequence of interference with $G\alpha_i$ proteins coupled to other receptors is still unclear and needs further investigation. The ACKR3-dependent increase in cAMP concentration resulted in PKA activation, as shown by our finding that all the CXCL12-induced nuclear effects were blocked by PKA inhibition.

The activation of PKA negatively regulates leukocyte adhesion by affecting the shedding of L-selectin, as well as the increased abundance and activation of integrins (*45*). By exploiting mouse models of intestinal inflammation, it has been demonstrated that in neutrophils, PKA activity increases gradually during adhesion to endothelial cells and transmigration (*27*). Moreover, during leukocyte TEM, PKA activation increases also in endothelial cells as a consequence of CD99 signaling (*46*). Consistent with previous studies (*27*, *47*), we found that PKA activity was not necessary for neutrophil migration through naked Boyden chambers, because PKA inhibition did not affect chemotaxis toward fMLP. However, PKA inhibition significantly reduced the number of neutrophils migrating through an endothelial layer toward fMLP by affecting the kinetics of cell migration. These results indicate that PKA is required for the ability of neutrophils to migrate through gaps between endothelial cells, supporting the idea that the CXCL12-ACKR3-PKA axis favors neutrophil migration only in dense microenvironments by triggering the deformation of the nucleus to

efficiently overcome physical barriers. PKA directly phosphorylates monomeric actin, substantially reducing the capacity of monomers to polymerize in vitro. In addition, PKA-mediated phosphorylation of vasodilator-stimulated phosphoprotein decreases its ability to nucleate, bind, and bundle actin filaments. Because we did not determine a substantial contribution of the actin cytoskeleton to CXCL12-induced nuclear reshaping, it is likely that the molecular target of PKA that regulates nuclear plasticity is located on or within the nucleus itself.

Nuclear stiffness increases with lamin A/C content, increased lamin A abundance impedes nuclear remodeling under mechanical stress (*48*), and lamin A/C phosphorylation precedes its turnover and nuclear softening in mesenchymal stromal cells (*49*). Furthermore, increased amounts of lamin A substantially reduced the ability of neutrophil-like HL-60 cells to pass through micrometer-scale constrictions (*4*) and prevent their motility through collagen I matrices (*7*). However, in comparison with that of HL-60 cells, the nuclear envelope of human blood neutrophil contains low-to-negligible amounts of several nuclear envelope proteins, including lamin A/C (*28*). Chromatin organization also plays a key role in cellular responses and adaptation to external mechanical cues. Studies of single, isolated nuclei showed that chromatin and lamins determine two different mechanical response regimes of the cell nucleus, such that lamin A/C abundance controls nuclear strain stiffening at large extensions, whereas chromatin governs the response to small extensions (*50*). Functionally, the efficient migration of B16-F1 melanoma cells (*51*), as well as the 3D migration of Jurkat cells (*29*), requires chromatin condensation. Specifically, the nuclei of mature mouse neutrophils show increased amounts of chromatin condensation markers (*30*). Here, we showed that the CXCL12-ACKR3-PKA axis induced changes in chromatin, promoting H4K20 dimethylation and nuclear compaction to sustain 3D cellular migration. The H4K20me2 mark is found throughout the nucleus and affects chromatin conformation and the DNA damage response. H4K20me2 is required for the efficient recruitment of XPA and 53BP1 to sites of DNA damage to repair double-strand breaks. Studies of HL-60 cells showed that confined cellular migration through a 5-μm pore induces transcriptional changes, which mainly affect the organization of inactive chromatin to protect active chromatin from disruption during squeezing (*52*). Therefore, it is likely that chemokine signals provide migratory advantages through complex environments by also protecting chromatin during 3D cellular migration.

In mammals, H4K20 methylation depends on three known enzymes: PR-Set7 (Set8) is responsible for generating H4K20me1, Suv420H1 catalyzes the generation of H4K20me2, and Suv420H2 catalyzes the generation of H4K20me3. Furthermore, although some enzymes involved in histone methylation are targets of PKA activity (*53*), whether Suv420H1 is directly phosphorylated by PKA needs further investigation. The discovery that chemokines can determine cell migration in dense microenvironments by regulating nuclear compaction might have multiple consequences in other research areas. CXCR4 and ACKR3 are expressed in T lymphocytes and in some metastatic tumor cells. Therefore, this research may pave the way to developing alternative strategies to control inflammation, facilitate leukocyte infiltration inside tumors, or limit cancer cell migration.

MATERIALS AND METHODS

Neutrophil purification

Mouse neutrophils were isolated from the bone marrow of healthy 8- to 12-week-old C57Bl6/J or LifeAct-GFP mice (*13*) using the Neutrophil Isolation Kit (Miltenyi Biotec) according to the manufacturer's instructions. Neutrophil purity was checked for every experiment by flow cytometry analysis of Ly6G-PE (phycoerythrin) (clone1A8; BD Pharmingen) and CD11b-PerCP Cy5.5 (clone M1/70; BD Pharmingen) with a FACSCanto II flow cytometer (BD Biosciences). The cell population obtained was routinely 90 to 95% pure neutrophils. C57BL/6J mice were purchased from Charles River Laboratories (Calco, Italy) and maintained under a 12-hour:12-hour light-dark cycle with food and water available ad libitum under specific pathogen–free conditions. LifeAct-GFP mice were a gift from A. M. Lennon-Dùmenil (Institut Curie, Paris, France) and the laboratory of F. Sepulveda (Institut Imagine, Paris, France). All experiments were approved and compliant with ethical regulations regarding animal research. The protocol was approved on 26 October 2016 by the Italian Ministry of Health (protocol no. 1045/2016-PR). Human granulocytes were isolated from the buffy coats of healthy volunteers by Ficoll-Paque gradient, which was followed by dextran sedimentation and hypotonic lysis of erythrocytes under endotoxin-free conditions. Purity was assessed by flow cytometry analysis of CD11b-PerCP Cy5.5 (clone M1/70; BD Pharmingen), CD15 (clone W6D3; BD Pharmingen), CD14 (clone M5E2; BD Pharmingen), and CD16 (clone 3G8, BD Pharmingen). Samples were acquired with a FACSCanto II flow cytometer (BD Biosciences) and analyzed with FlowJo software.

Cell migration through 3D collagen gels

Freshly purified mouse neutrophils were mixed at 4°C with rat tail collagen type I (4 mg/ml at basic pH; Corning) and loaded in a custom-made chamber in PDMS. The samples were incubated at 37°C for 20 min to allow gel polymerization before 2 ml of RPMI (EuroClone) supplemented with 10% fetal bovine serum (FBS; Euroclone) and granulocyte-macrophage colony-stimulating factor (GM-CSF; 50 ng/ml; Miltenyi Biotech) and containing CXCL12 (40 ng/ml; R&D Systems) was added to the dish. Where indicated in the figure legends, cells were preincubated for 1 hour with AMD3100 (10 μg/ml; Sigma-Aldrich), 100 nM CCX771 (Chemocentryx), PTx (100 ng/ml; Sigma-Aldrich), 1 μM myr-PKI (Enzo Life Sciences), or 14 μM A-196 (Sigma-Aldrich) before chemokine was added, and these compounds were maintained or not in the medium during cell migration. Cells were imaged for 5 hours with a DMi8 inverted microscope (Leica) at 37°C with a 5% CO_2 atmosphere and a 10× dry objective lens (numerical aperture 0.40 phase). Trajectories of cells moving for 1 hour after CXCL12 was added were obtained upon tracking with Imaris software. Tracks of objects that moved <5 μm in length or for <5 min were removed from the analysis to avoid artifacts. Computational analyses of these trajectories were performed using in-house Python algorithms. Instantaneous speed was computed for each time point and for each cell during the duration of the movie. To quantitatively describe cell motility, we computed the MSD, which is an established indicator of the spatial extent of a set of trajectories. The MSD is defined as the average over all the trajectories of the squared distance traveled during a certain time lag, *t*. To illustrate

cell displacement, we show a random sample of trajectories of duration t together with a circle of radius that equals the square root of the MSD at time t (noted as r). Directionality was defined as the proportion of the velocity (v) directed toward the chemokine source; that is, if x is an axis directed toward the chemokine source, then the directionality will be (vx/v). By this definition, directionality also coincides with the cosine of the angle between cell speed and the chemokine gradient.

Analysis of cell size and nuclear size in collagen gels

Suspensions of purified LifeAct-GFP neutrophils (1×10^6 cells/ml) were serum starved for 30 min at 37°C with a 5% CO_2 in RPMI (EuroClone) supplemented with 0.1% FBS (Euroclone), before undergoing stimulation with CXCL12 (40 ng/ml; R&D Systems) and counterstaining with Hoechst (200 ng/ml; Life Technologies) at 37°C for 30 min. Mixes of carboxytetramethylrhodamine (TAMRA)-fluorescent rat tail collagen type I (BD Biosciences) and RPMI–0.1% FBS medium were prepared with collagen at a final concentration of 4 mg/ml. Neutrophils were added to the collagen mixtures, which were deposited in custom-made PDMS-based collagen chambers and incubated at 37°C for 20 min to enable collagen polymerization. Neutrophils were then left to adapt and migrate within the 3D environment at 37°C for 2 hours. After undergoing a wash with phosphate-buffered saline (PBS; Euroclone), the cells were fixed for 1 hour with 4% paraformaldehyde (PFA). Confocal images were acquired with a spinning disk microscope (Leica DMi8 equipped with a CSU-X1 Confocal Scanner Unit) with a 40× dry objective. Relative cell and nuclear sizes were estimated with the Fiji 3D Object Counter plugin to measure volume. Data were normalized relative to untreated neutrophils (set at 100%). To calculate the pore size of the collagen meshwork, we corrected images by local background subtraction with a rolling ball algorithm (48-pixel radius). A median filter (noise despeckle) was then applied for random noise removal. The resulting images were binarized with a threshold segmentation based on the triangle algorithm. All pixels corresponding to the collagen fibers were set to 1 and the remainder was set to 0 (fluid phase). From there, a Euclidean distance map (EDM) was derived, specifying for every fluid pixel its distance to the nearest collagen pixel. The average distance between a fluid pixel and collagen pixel was extracted from the EDM distribution and then multiplied by 2 to obtain the pore size.

Gene expression analysis

Microarray gene expression data were generated by the Immunological Genome Project (*31*), requested on 12 January 2019 from its website. Neutrophils and classical monocytes corresponded to myeloid cells sorted according to their immunophenotype. Classical monocytes from bone marrow are $B220^-CD43^-CD115^+Ly\text{-}6C^+MHCII^-$; classical monocytes from blood are $B220^-CD3^-CD115^+Ly\text{-}6C^+MHCII^-$; neutrophils from bone marrow are $CD11b^+Gr1{+}7/4hi$; neutrophils from blood are $CD11b^+Ly6\text{-}G^+$. Data analysis and visualization were performed with an in-house code in Python 3 with the libraries panda, matplotlib, and seaborn. Each gene expression value could be retrieved with the online data browser Gene Skyline of Immgen (www.immgen.org).

Cell migration in microchannels and through microconstrictions

PDMS (GE Silicones) was used to prepare 8 × 5 μm microchannels with 1-μm side constrictions from a custom-made mold. The PDMS chamber and a 35-mm glass-bottom dish (FD35-100, WPI) were plasma activated before being bound to each other. The binding was left to strengthen in a 65°C oven for 1 hour. The microchannels were then plasma cleaned, coated with fibronectin (10 μg/ml; Sigma-Aldrich) at room temperature for 1 hour, and then washed three times with PBS before cell loading (*14*). Purified neutrophil suspensions (1×10^6 cells/ml) were serum starved for 30 min at 37°C with 5% CO_2 in RPMI (EuroClone) supplemented with 0.1% bovine serum albumin (BSA) before being incubated with CXCL12 (40 ng/ml; R&D Systems) and undergoing Hoechst counterstaining (200 ng/ml; Life Technologies) at 37°C for 30 min. The cells were then washed and resuspended in RPMI medium supplemented with 10% FBS and GM-CSF (50 ng/ml; Miltenyi Biotech) to be deposited in the chamber entry pores. Where indicated in the figure legends, neutrophils were treated with AMD3100 (10 μg/ml for 30 min; Sigma-Aldrich), CCX771 (100 nM for 10 min; Chemocentryx), or myr-PKI (1 μM for 30 min; Enzo Life Sciences) both before incubation with CXCL12 and during the recording. Migrating neutrophils were imaged for 6 hours on an epifluorescence microscope (Leica DMi8, Leica Microsystems) equipped with a cooled charge-coupled device camera (HQ2, Photometrics) with a 10× objective. We focused on the passing of the first constriction encountered by the cell. Analysis of the velocity of neutrophil migration was performed with a custom-made, semiautomatized ImageJ macro (*14*). The percentage of passage through microconstrictions was calculated as the ratio between the number of cells that passed a constriction and the number of cells that encountered a constriction. PDMS-based 3 × 4 μm microchannels were used to visualize the actin cytoskeleton during confined migration of LifeAct-GFP neutrophils. Analysis of cell speed, nuclear aspect ratio, and circularity was performed with ImageJ software. The amount of actin behind the nucleus in migratory cells was calculated as previously described (*15*). Briefly, the nucleus was contained in the first third of each cell. Thus, we calculated the amount of LifeAct-GFP signal in the last 66% of the cell, which was divided by the amount of actin in the first 33% (nuclear area). This provided a back:front ratio per cell, which was indicative of the overall distribution of the actin cytoskeleton per cell under each condition.

Micropillar fabrication

Custom-made PDMS (Sylgard 184, Dow-Corning, Midland, MI) microstructured substrates were fabricated through a replica-molding process. As the first step, the negative pattern was prepared through standard photolithography technique: Si wafers were photopatterned with an AZ-1518 negative photoresist (MicroChemicals, Germany). The obtained microstructured Si wafers were subsequently silanized to facilitate PDMS removal during the replica-molding step. PDMS elastomer was thoroughly mixed with the silicone elastomer curing agent in a 10:1 ratio, poured over the microstructured Si master, cured at 80°C for 1 hour, and subsequently peeled off the Si wafers. The height of the microstructures was fixed at about 7 μm. Micropillar substrates were punched with a 5-mm-diameter biopsy punch and sterilized in an autoclave. Substrates were plasma treated for 2 min and positioned in a 96 multiwell and then covered with 50 μl of sterile poly-L-lysine (50

μg/ml; Sigma-Aldrich) and fibronectin (10 μg/ml; Sigma-Aldrich) (*17*).

Nuclear deformability assay

Purified C57Bl6/J mouse neutrophil suspensions (1×10^6 cells/ml) were serum starved for 30 min at 37°C with 5% CO_2 in RPMI (EuroClone) supplemented with 0.1% BSA, before stimulation with CXCL12 (40 ng/ml; R&D Systems) at 37°C for 30 min. Where indicated in the figure legends, cells were pretreated before CXCL12 exposure with the following compounds for the specified incubation times: AMD3100 (10 μg/ml for 30 min; Sigma-Aldrich), CCX771 (100 nM for 10 min; Chemocentryx), PTx (100 ng/ml for 30 min; Sigma-Aldrich), or myr-PKI (1 μM for 30 min; Enzo Life Sciences). Cells were then left unexposed or were exposed to chemokines for 30 min at 37°C and then seeded on fibronectin-coated, custom-made pillar substrates (10 μg/ml; Sigma-Aldrich) and cultured for 1 hour in a humidified incubator at 37°C with 5% CO_2. CXCL12 (R&D Systems), CXCL11_12 chimera (*25*), and CXCL11 (R&D Systems) were used at a final concentration of 40 ng/ml, whereas cells were treated with 10 μM forskolin (Sigma-Aldrich) for 30 min. Micropillar samples were then fixed with 4% PFA for 30 min and stained for F-actin with Phalloidin–Alexa Fluor 488 (Life Technologies). Neutrophil nuclei were counterstained with Hoechst 33342 (Life Technologies) and mounted on glass slides with Prolong antifade reagent (Life Technologies). Cells were visualized with a 40× oil immersion objective on a laser-scanning confocal microscope (Leica TCS-SP5, Leica Microsystems). Images were analyzed with an algorithm developed in the laboratory using the MATLAB platform. The algorithm counts the number of nuclear pixels between the medians and the maximal values of intensity range of each image stack. The nuclear volume distribution along the vertical axis of micropillars was calculated as the percentage of the Hoechst-positive pixels at the top and bottom of the micropillars. We considered the percentage of nuclear content embedded at the bottom of the micropillars as an index of nuclear deformability.

RNA extraction and real-time PCR

Total RNA was extracted from freshly purified neutrophils or neutrophils kept in culture for 3 hours in RPMI and 10% FBS with TRIzol reagent (Thermo Fisher Scientific). Complementary DNA was synthetized from 100 to 200 ng of RNA with the High-Capacity RT Kit (Applied Biosystems) according to the manufacturer's instructions. Real-time PCR was performed with SYBR Green I (Applied Biosystems) on a 7900HT Fast Real-Time PCR System (Applied Biosystems) with the following primers: *Cxcr4* (forward: 5′-TCAGTGGCTGACCTCCTCTT-3′; reverse: 5′-CTTGGCCTTTGACTGTTGGT-3′), *Ackr3* (forward: 5′-CTTGGCCTTTGACTGTTGGT-3′; reverse: 5′-GTGCCGGTGAAGTAGGTGAT-3′), and *Gapdh* (forward: 5′-GCAAAGTGGAGATTGTTGCCA-3′; reverse: 5′-CCTTGACTGTGCCGTTGAATTT-3′). The expression of a gene of interest was normalized to that of *Gapdh*.

Flow cytometry

Neutrophils isolated from the bone marrow of healthy 8- to 12-week-old C57Bl6/J mice with the Neutrophil Isolation Kit (Miltenyi Biotec) were stained with anti-Ly6G Pacific Blue (clone 1A8; BD Pharmingen) and CD11b-PerCP Cy5.5 (clone M1/70; BD Pharmingen). Intracellular staining for ACKR3 was performed with the BD Cytofix/Cytoperm Kit and PE-conjugated anti-human/mouse CXCR7 antibody (clone 8F11-M16, BioLegend). Samples were analyzed with a Cytoflex flow cytometer equipped with 405-, 488-, and 638-nm lasers (Beckman Coulter Inc., CA, USA) and analyzed with FlowJo software.

Immunogold and transmission electron microscopy

Purified C57Bl6/J neutrophil suspensions were fixed with PBS and 4% PFA, dehydrated, embedded in LR White Resin, and polymerized at 58°C. Ultrathin sections were placed on formvar-coated nickel grids and used the next day for immunogold labeling. For electron immunostaining of sections for electron microscopy, the postembedding immunogold method was applied. Ultrathin sections were first treated with blocking solution (0.5% BSA, 0.1% Triton X, and 1× PBS) and then incubated with PE-conjugated anti-human/mouse CXCR7 antibody (diluted 1:4; clone 8F11-M16, BioLegend) overnight at 4°C. Antibody binding was detected with anti-mouse immunoglobulin G (diluted 1:100; Sigma-Aldrich, G7402) coupled to gold particles of 10 nm diameter. Sections were analyzed with a FEI Tecnai G12 transmission electron microscope operating at 100 kV. The images were captured with a Veleta digital camera (Olympus Soft Imaging System). For control samples, primary antibody was omitted.

cAMP measurement

Neutrophils purified from bone marrow were preincubated with AMD3100 (10 μg/ml; Sigma-Aldrich) for 30 min at 37°C with 5% CO_2. Subsequently, 3×10^6 cells were left untreated or were treated with CXCL12 (40 ng/ml) for 5 min. The phosphodiesterase inhibitor 3-isobutyl-1-methylxanthine (IBMX; 100 μM; Sigma-Aldrich) and the adenylyl cyclase stimulant forskolin (10 μM; Sigma-Aldrich) were used as positive controls. Cells were then washed and centrifuged at 300*g* for 10 min at room temperature. The supernatants were removed, and the cells were lysed in 330 μl of 0.1 M HCl by sonication for 10 min. To measure the concentration of intracellular cAMP, we used a cAMP Complete ELISA (enzyme-linked immunosorbent assay) Kit (KA0320, Abnova) was used according to the manufacturer's instructions. Data were normalized to the amount of protein of the cell lysate, which was quantified with the Quantum Protein Assay Kit (EuroClone).

Immunofluorescence microscopy

Neutrophils purified from bone marrow were seeded on Cell Culture Slides (Falcon) in RPMI–0.1% FBS for 30 min before chemokine stimulation. Cells were stimulated with CXCL12 (40 ng/ml), CXCL11_12 (40 ng/ml), and forskolin (10 μM) for 30 min and then fixed with 4% PFA for 10 min at room temperature. Cells were permeabilized with 0.1% Triton X for 10 min and stained with anti-H4K20me2 antibody (Abcam) overnight at 4°C. After washing, the appropriate anti-rabbit secondary antibody was used (Life Technologies). Samples were stained with Phalloidin–Alexa Fluor 488 (Life Technologies) for actin and with Hoechst 33342 for nuclear counterstaining and then mounted with ProLong (Invitrogen). Images were acquired with a laser-scanning confocal microscope (Leica TCS-SP5, Leica Microsystems) using a 63× oil objective. Analysis of fluorescence intensity and surface areas was performed using ImageJ software.

Chemotaxis assay

Neutrophils purified from bone marrow (1×10^6 cells/ml) were serum starved for 30 min at 37°C with 5% CO_2 in RPMI (EuroClone) supplemented with 0.1% BSA before preincubation with AMD3100 (10 μg/ml for 30 min; Sigma-Aldrich), CCX771 (100 nM for 10 min; Chemocentryx), or myr-PKI (1 μM for 30 min; Enzo Life Sciences). The neutrophils were then seeded in the upper chamber of a 3-μm-pore size Transwell plate (Corning). The lower chambers were filled with medium alone or medium containing CXCL12 (40 ng/ml) or fMLP (1 μM; Sigma-Aldrich). After 1 hour of incubation at 37°C, the number of cells that had migrated into the lower chamber was estimated with a FACSCanto II flow cytometer (BD Biosciences).

TEM assay

TEM assays were performed with 24-well plates with microporous (3-μm) Transwell membrane inserts (Corning; Costar) coated with SVEC4-10 cells [American Type Culture Collection (ATCC) #CRL-2181, Manassas, VA], an endothelial cell line from murine axillary lymph nodes. SVEC4-10 cells were cultured in Dulbecco's modified Eagle's medium (ATCC 30-2002, Manassas, VA) supplemented with 10% FBS (Gibco), penicillin, and streptomycin in a humidified incubator at 37°C with 5% CO_2. SVEC4-10 cells (1×10^5) were seeded in the top chamber of the transwell inserts and incubated overnight at 37°C. SVEC4-10 monolayers were then activated with tumor necrosis factor–α (50 ng/ml; Peprotech) for 4 hours. Purified neutrophils (1×10^6 cells/ml) were serum starved for 30 min at 37°C with 5% CO_2 in RPMI (EuroClone) supplemented with 0.1% BSA before preincubation with AMD3100 (10 μg/ml for 30 min; Sigma-Aldrich), CCX771 (100 nM for 10 min; Chemocentryx), myr-PKI (1 μM for 30 min; Enzo Life Sciences), or A-196 (14 μM; Sigma-Aldrich). Neutrophils (2×10^5 cells) were added on top of the transwells, whereas assay medium (600 μl) with or without 1 μM fMLP (Sigma-Aldrich) was added to the bottom chambers. After 1 hour of incubation at 37°C, transmigration was assessed by counting the number of cells in the bottom chambers with a FACSCanto II flow cytometer (BD Biosciences).

Static adhesion assay

Neutrophils purified from bone marrow were suspended at a density of 5×10^6/ml in standard adhesion buffer [PBS, 10% FBS, 1 mM $CaCl_2$, and 1 mM $MgCl_2$ (pH 7.2)]. Adhesion assays were performed on 18-well glass slides coated with murine ICAM-1 (1 μg/ml) in PBS. Cell suspension (20 μl) was added to the well and incubated at 37°C for 3 min with 5 μl of CXCL12 (2 μg/ml). After washing, the adherent cells were fixed in 1.5% glutaraldehyde in ice-cold PBS and counted by computer-assisted enumeration.

Western blotting

Freshly purified bone marrow mouse neutrophils or mouse bone marrow–derived dendritic cells (1×10^6 cells) were lysed in Cell Extraction Buffer (FNN0011, Thermo Fisher Scientific) containing protease and phosphatase inhibitor cocktail (Halt Protease and Phosphatase Inhibitor Cocktail, Thermo Fisher Scientific) at 4°C for 20 min. Proteins were resuspended in Laemmli sample buffer, separated by electrophoresis on a 4 to 12% precast Bis-Tris Protein Gel (Thermo Fisher Scientific), and transferred onto nitrocellulose membranes (Thermo Fisher Scientific). Blots were incubated with primary antibodies against lamin A (1:1000; 4C11, Cell Signaling Technology), lamin B1 [1:1000; EPR8985(B), Abcam], histone H4 (1:1000; Abcam), and Suv420H1 (1:500; Abcam) overnight at 4°C and then were incubated with the appropriate peroxidase-conjugated secondary antibodies (Bio-Rad). Blots were developed with SuperSignal West Pico PLUS Chemiluminescent Substrate (Thermo Fisher Scientific) on the ChemiDoc MP System (Bio-Rad).

Statistical analysis

All of the images shown in the figures correspond to representative experiments in which the number of cells analyzed is indicated by "n" in the legends. Each experiment was repeated N times, as specified in the figure legends. There were no preestablished criteria for sample exclusion, except evident technical damage in microfabricated devices. Investigators were mostly blinded to sample allocation during experiments. Data were analyzed with Prism Software (GraphPad, La Jolla, CA, USA). In general, statistical comparison between two groups was performed with the Mann-Whitney test. For multiple comparisons, the Kruskal-Wallis test was performed. Results with $P < 0.05$ were considered to be statistically significant. In figures, asterisks are used as follows: $^*P < 0.05$, $^{**}P < 0.01$, $^{***}P < 0.001$, and $^{****}P < 0.0001$.

Supplementary Materials

This PDF file includes:
Figs. S1 to S7

Other Supplementary Material for this manuscript includes the following:
MDAR Reproducibility Checklist
Movies S1 to S5

View/request a protocol for this paper from *Bio-protocol*.

REFERENCES AND NOTES

1. S. Nourshargh, P. L. Hordijk, M. Sixt, Breaching multiple barriers: Leukocyte motility through venular walls and the interstitium. *Nat. Rev. Mol. Cell Biol.* **11**, 366–378 (2010).
2. L. A. Lautscham, C. Kämmerer, J. R. Lange, T. Kolb, C. Mark, A. Schilling, P. L. Strissel, R. Strick, C. Gluth, A. C. Rowat, C. Metzner, B. Fabry, Migration in confined 3D environments is determined by a combination of adhesiveness, nuclear volume, contractility, and cell stiffness. *Biophys. J.* **109**, 900–913 (2015).
3. J. Lammerding, Mechanics of the nucleus. *Compr. Physiol.* **1**, 783–807 (2011).
4. A. C. Rowat, D. E. Jaalouk, M. Zwerger, W. L. Ung, I. A. Eydelnant, D. E. Olins, A. L. Olins, H. Herrmann, D. A. Weitz, J. Lammerding, Nuclear envelope composition determines the ability of neutrophil-type cells to passage through micron-scale constrictions. *J. Biol. Chem.* **288**, 8610–8618 (2013).
5. M. Salvermoser, R. Pick, L. T. Weckbach, A. Zehrer, P. Löhr, M. Drechsler, M. Sperandio, O. Soehnlein, B. Walzog, Myosin 1f is specifically required for neutrophil migration in 3D environments during acute inflammation. *Blood* **131**, 1887–1898 (2018).
6. S. K. Yadav, D. Stojkov, S. W. Feigelson, F. Roncato, H.-U. Simon, S. Yousefi, R. Alon, Chemokine-triggered microtubule polymerization promotes neutrophil chemotaxis and invasion but not transendothelial migration. *J. Leukoc. Biol.* **105**, 755–766 (2019).
7. S. K. Yadav, S. W. Feigelson, F. Roncato, M. Antman-Passig, O. Shefi, J. Lammerding, R. Alon, Frontline science: Elevated nuclear lamin A is permissive for granulocyte transendothelial migration but not for motility through collagen I barriers. *J. Leukoc. Biol.* **104**, 239–251 (2018).
8. M. J. Delano, K. M. Kelly-Scumpia, T. C. Thayer, R. D. Winfield, P. O. Scumpia, A. G. Cuenca, P. B. Harrington, K. A. O'Malley, E. Warner, S. Gabrilovich, C. E. Mathews, D. Laface, P. G. Heyworth, R. Ramphal, R. M. Strieter, L. L. Moldawer, P. A. Efron, Neutrophil mobilization from the bone marrow during polymicrobial sepsis is dependent on CXCL12 signaling. *J. Immunol.* **187**, 911–918 (2011).

9. K. J. Eash, J. M. Means, D. W. White, D. C. Link, CXCR4 is a key regulator of neutrophil release from the bone marrow under basal and stress granulopoiesis conditions. *Blood* **113**, 4711–4719 (2009).
10. L. Barbier, P. J. Sáez, R. Attia, A. M. Lennon-Duménil, I. Lavi, M. Piel, P. Vargas, Myosin II activity is selectively needed for migration in highly confined microenvironments in mature dendritic cells. *Front. Immunol.* **10**, 747 (2019).
11. P. J. Saez, L. Barbier, R. Attia, H.-R. Thiam, M. Piel, P. Vargas, Leukocyte migration and deformation in collagen gels and microfabricated constrictions. *Methods Mol. Biol.* **1749**, 361–373 (2018).
12. S. Sormendi, M. Deygas, A. Sinha, M. Bernard, A. Krüger, I. Kourtzelis, G. le Lay, P. J. Sáez, M. Gerlach, K. Franke, A. Meneses, M. Kräter, A. Palladini, J. Guck, Ü. Coskun, T. Chavakis, P. Vargas, B. Wielockx, HIF2α is a direct regulator of neutrophil motility. *Blood* **137**, 3416–3427 (2021).
13. J. Riedl, K. C. Flynn, A. Raducanu, F. Gärtner, G. Beck, M. Bösl, F. Bradke, S. Massberg, A. Aszodi, M. Sixt, R. Wedlich-Söldner, Lifeact mice for studying F-actin dynamics. *Nat. Methods* **7**, 168–169 (2010).
14. P. Vargas, P. Maiuri, M. Bretou, P. J. Sáez, P. Pierobon, M. Maurin, M. Chabaud, D. Lankar, D. Obino, E. Terriac, M. Raab, H.-R. Thiam, T. Brocker, S. M. Kitchen-Goosen, A. S. Alberts, P. Sunareni, S. Xia, R. Li, R. Voituriez, M. Piel, A.-M. Lennon-Duménil, Innate control of actin nucleation determines two distinct migration behaviours in dendritic cells. *Nat. Cell Biol.* **18**, 43–53 (2016).
15. H. R. Thiam, P. Vargas, N. Carpi, C. L. Crespo, M. Raab, E. Terriac, M. C. King, J. Jacobelli, A. S. Alberts, T. Stradal, A.-M. Lennon-Dumenil, M. Piel, Perinuclear Arp2/3-driven actin polymerization enables nuclear deformation to facilitate cell migration through complex environments. *Nat. Commun.* **7**, 10997 (2016).
16. P. M. Davidson, O. Fromigué, P. J. Marie, V. Hasirci, G. Reiter, K. Anselme, Topographically induced self-deformation of the nuclei of cells: Dependence on cell type and proposed mechanisms. *J. Mater. Sci. Mater. Med.* **21**, 939–946 (2010).
17. E. Grespan, G. G. Giobbe, F. Badique, K. Anselme, J. Rühe, N. Elvassore, Effect of geometrical constraints on human pluripotent stem cell nuclei in pluripotency and differentiation. *Integr Biol (Camb)* **10**, 278–289 (2018).
18. K. Balabanian, B. Lagane, S. Infantino, K. Y. C. Chow, J. Harriague, B. Moepps, F. Arenzana-Seisdedos, M. Thelen, F. Bachelerie, The chemokine SDF-1/CXCL12 binds to and signals through the orphan receptor RDC1 in T lymphocytes. *J. Biol. Chem.* **280**, 35760–35766 (2005).
19. J. C. Gutjahr, K. S. Crawford, D. R. Jensen, P. Naik, F. C. Peterson, G. P. B. Samson, D. F. Legler, J. Duchene, C. T. Veldkamp, A. Rot, B. F. Volkman, The dimeric form of CXCL12 binds to atypical chemokine receptor 1. *Sci. Signal.* **14**, eabc9012 (2021).
20. R. D. Berahovich, B. A. Zabel, M. E. T. Penfold, S. Lewén, Y. Wang, Z. Miao, L. Gan, J. Pereda, J. Dias, I. I. Slukvin, K. E. McGrath, J. C. Jaen, T. J. Schall, CXCR7 protein is not expressed on human or mouse leukocytes. *J. Immunol.* **185**, 5130–5139 (2010).
21. T. N. Hartmann, V. Grabovsky, R. Pasvolsky, Z. Shulman, E. C. Buss, A. Spiegel, A. Nagler, T. Lapidot, M. Thelen, R. Alon, A crosstalk between intracellular CXCR7 and CXCR4 involved in rapid CXCL12-triggered integrin activation but not in chemokine-triggered motility of human T lymphocytes and $CD34^+$ cells. *J. Leukoc. Biol.* **84**, 1130–1140 (2008).
22. H.-Y. Kim, S.-Y. Lee, D.-Y. Kim, J.-Y. Moon, Y.-S. Choi, I.-C. Song, H.-J. Lee, H.-J. Yun, S. Kim, D.-Y. Jo, Expression and functional roles of the chemokine receptor CXCR7 in acute myeloid leukemia cells. *Blood Res.* **50**, 218–226 (2015).
23. F. M. Konrad, N. Meichssner, A. Bury, K. C. Ngamsri, J. Reutershan, Inhibition of SDF-1 receptors CXCR4 and CXCR7 attenuates acute pulmonary inflammation via the adenosine A2B-receptor on blood cells. *Cell Death Dis.* **8**, e2832 (2017).
24. B. A. Zabel, S. Lewen, R. D. Berahovich, J. C. Jaen, T. J. Schall, The novel chemokine receptor CXCR7 regulates trans-endothelial migration of cancer cells. *Mol. Cancer* **10**, 73 (2011).
25. R. Ameti, S. Melgrati, E. Radice, E. Cameroni, E. Hub, S. Thelen, A. Rot, M. Thelen, Characterization of a chimeric chemokine as a specific ligand for ACKR3. *J. Leukoc. Biol.* **104**, 391–400 (2018).
26. A. Levoye, K. Balabanian, F. Baleux, F. Bachelerie, B. Lagane, CXCR7 heterodimerizes with CXCR4 and regulates CXCL12-mediated G protein signaling. *Blood* **113**, 6085–6093 (2009).
27. R. Mizuno, Y. Kamioka, K. Kabashima, M. Imajo, K. Sumiyama, E. Nakasho, T. Ito, Y. Hamazaki, Y. Okuchi, Y. Sakai, E. Kiyokawa, M. Matsuda, In vivo imaging reveals PKA regulation of ERK activity during neutrophil recruitment to inflamed intestines. *J. Exp. Med.* **211**, 1123–1136 (2014).
28. A. L. Olins, M. Zwerger, H. Herrmann, H. Zentgraf, A. J. Simon, M. Monestier, D. E. Olins, The human granulocyte nucleus: Unusual nuclear envelope and heterochromatin composition. *Eur. J. Cell Biol.* **87**, 279–290 (2008).
29. P. Wang, M. Dreger, E. Madrazo, C. J. Williams, R. Samaniego, N. W. Hodson, F. Monroy, E. Baena, P. Sánchez-Mateos, A. Hurlstone, J. Redondo-Muñoz, WDR5 modulates cell motility and morphology and controls nuclear changes induced by a 3D environment. *Proc. Natl. Acad. Sci. U.S.A.* **115**, 8581–8586 (2018).
30. D. E. Olins, A. L. Olins, Granulocyte heterochromatin: Defining the epigenome. *BMC Cell Biol.* **6**, 39 (2005).
31. T. S. P. Heng, M. W. Painter; Immunological Genome Project Consortium, The Immunological Genome Project: Networks of gene expression in immune cells. *Nat. Immunol.* **9**, 1091–1094 (2008).
32. K. D. Bromberg, T. R. H. Mitchell, A. K. Upadhyay, C. G. Jakob, M. A. Jhala, K. M. Comess, L. M. Lasko, C. Li, C. T. Tuzon, Y. Dai, F. Li, M. S. Eram, A. Nuber, N. B. Soni, V. Manaves, M. A. Algire, R. F. Sweis, M. Torrent, G. Schotta, C. Sun, M. R. Michaelides, A. R. Shoemaker, C. H. Arrowsmith, P. J. Brown, V. Santhakumar, A. Martin, J. C. Rice, G. G. Chiang, M. Vedadi, D. Barsyte-Lovejoy, W. N. Pappano, The SUV4-20 inhibitor A-196 verifies a role for epigenetics in genomic integrity. *Nat. Chem. Biol.* **13**, 317–324 (2017).
33. K. De Filippo, S. M. Rankin, CXCR4, the master regulator of neutrophil trafficking in homeostasis and disease. *Eur. J. Clin. Invest.* **48** (Suppl. 2), e12949 (2018).
34. M. Casanova-Acebes, C. Pitaval, L. A. Weiss, C. Nombela-Arrieta, R. Chèvre, N. A-González, Y. Kunisaki, D. Zhang, N. van Rooijen, L. E. Silberstein, C. Weber, T. Nagasawa, P. S. Frenette, A. Castrillo, A. Hidalgo, Rhythmic modulation of the hematopoietic niche through neutrophil clearance. *Cell* **153**, 1025–1035 (2013).
35. B. A. Zabel, Y. Wang, S. Lewén, R. D. Berahovich, M. E. T. Penfold, P. Zhang, J. Powers, B. C. Summers, Z. Miao, B. Zhao, A. Jalili, A. Janowska-Wieczorek, J. C. Jaen, T. J. Schall, Elucidation of CXCR7-mediated signaling events and inhibition of CXCR4-mediated tumor cell transendothelial migration by CXCR7 ligands. *J. Immunol.* **183**, 3204–3211 (2009).
36. S. Rajagopal, J. Kim, S. Ahn, S. Craig, C. M. Lam, N. P. Gerard, C. Gerard, R. J. Lefkowitz, Beta-arrestin- but not G protein-mediated signaling by the "decoy" receptor CXCR7. *Proc. Natl. Acad. Sci. U.S.A.* **107**, 628–632 (2010).
37. R. L. Contento, B. Molon, C. Boularan, T. Pozzan, S. Manes, S. Marullo, A. Viola, CXCR4-CCR5: A couple modulating T cell functions. *Proc. Natl. Acad. Sci. U.S.A.* **105**, 10101–10106 (2008).
38. B. Molon, G. Gri, M. Bettella, C. Gómez-Moutón, A. Lanzavecchia, C. Martínez-A, S. Mañes, A. Viola, T cell costimulation by chemokine receptors. *Nat. Immunol.* **6**, 465–471 (2005).
39. D. Sohy, M. Parmentier, J. Y. Springael, Allosteric transinhibition by specific antagonists in CCR2/CXCR4 heterodimers. *J. Biol. Chem.* **282**, 30062–30069 (2007).
40. L. J. Albee, J. M. Eby, A. Tripathi, H. M. LaPorte, X. Gao, B. F. Volkman, V. Gaponenko, M. Majetschak, α_1-Adrenergic receptors function within hetero-oligomeric complexes with atypical chemokine receptor 3 and chemokine (C-X-C motif) receptor 4 in vascular smooth muscle cells. *J. Am. Heart Assoc.* **6**, e006575 (2017).
41. X. Gao, H. Abdelkarim, L. J. Albee, B. F. Volkman, V. Gaponenko, M. Majetschak, Partial agonist activity of α1-adrenergic receptor antagonists for chemokine (C-X-C motif) receptor 4 and atypical chemokine receptor 3. *PLOS ONE* **13**, e0204041 (2018).
42. X. Jiao, P. J. Gonzalez-Cabrera, L. Xiao, M. E. Bradley, P. W. Abel, W. B. Jeffries, Tonic inhibitory role for cAMP in α_{1a}-adrenergic receptor coupling to extracellular signal-regulated kinases 1/2. *J. Pharmacol. Exp. Ther.* **303**, 247–256 (2002).
43. A. Scanzano, M. Cosentino, Adrenergic regulation of innate immunity: A review. *Front. Pharmacol.* **6**, 171 (2015).
44. G. D. LeSage, D. Alvaro, S. Glaser, H. Francis, L. Marucci, T. Roskams, J. L. Phinizy, M. Marzioni, A. Benedetti, S. Taffetani, B. Barbaro, G. Fava, Y. Ueno, G. Alpini, α-1 adrenergic receptor agonists modulate ductal secretion of BDL rats via Ca^{2+}- and PKC-dependent stimulation of cAMP. *Hepatology* **40**, 1116–1127 (2004).
45. M. J. Lorenowicz, M. Fernandez-Borja, P. L. Hordijk, cAMP signaling in leukocyte transendothelial migration. *Arterioscler. Thromb. Vasc. Biol.* **27**, 1014–1022 (2007).
46. R. L. Watson, J. Buck, L. R. Levin, R. C. Winger, J. Wang, H. Arase, W. A. Muller, Endothelial CD99 signals through soluble adenylyl cyclase and PKA to regulate leukocyte transendothelial migration. *J. Exp. Med.* **212**, 1021–1041 (2015).
47. L. Chavez-Vargas, S. R. Adame-García, R. D. Cervantes-Villagrana, A. Castillo-Kauil, J. G. H. Bruystens, S. Fukuhara, S. S. Taylor, N. Mochizuki, G. Reyes-Cruz, J. Vázquez-Prado, Protein kinase A (PKA) type I interacts with P-Rex1, a rac guanine nucleotide exchange factor: Effect on PKA localization and P-Rex1 signaling. *J. Biol. Chem.* **291**, 6182–6199 (2016).
48. T. Harada, J. Swift, J. Irianto, J.-W. Shin, K. R. Spinler, A. Athirasala, R. Diegmiller, P. C. D. P. Dingal, I. L. Ivanovska, D. E. Discher, Nuclear lamin stiffness is a barrier to 3D migration, but softness can limit survival. *J. Cell Biol.* **204**, 669–682 (2014).
49. A. Buxboim, J. Swift, J. Irianto, K. R. Spinler, P. C. D. P. Dingal, A. Athirasala, Y.-R. C. Kao, S. Cho, T. Harada, J.-W. Shin, D. E. Discher, Matrix elasticity regulates lamin-A,C phosphorylation and turnover with feedback to actomyosin. *Curr. Biol.* **24**, 1909–1917 (2014).
50. A. D. Stephens, E. J. Banigan, S. A. Adam, R. D. Goldman, J. F. Marko, Chromatin and lamin A determine two different mechanical response regimes of the cell nucleus. *Mol. Biol. Cell* **28**, 1984–1996 (2017).
51. G. Gerlitz, M. Bustin, Efficient cell migration requires global chromatin condensation. *J. Cell Sci.* **123**, 2207–2217 (2010).

52. E. C. Jacobson, J. K. Perry, D. S. Long, A. L. Olins, D. E. Olins, B. E. Wright, M. H. Vickers, J. M. O'Sullivan, Migration through a small pore disrupts inactive chromatin organization in neutrophil-like cells. *BMC Biol.* **16**, 142 (2018).
53. A. Baba, F. Ohtake, Y. Okuno, K. Yokota, M. Okada, Y. Imai, M. Ni, C. A. Meyer, K. Igarashi, J. Kanno, M. Brown, S. Kato, PKA-dependent regulation of the histone lysine demethylase complex PHF2-ARID5B. *Nat. Cell Biol.* **13**, 668–675 (2011).

Acknowledgments: We thank T. Pozzobon for the help with the micropillar experiments; the DeBioImaging Facility, Department of Biology, for electron microscopy; and R. Angioni for helping with FACS. We also thank C. Faliti, K. Lefkimmiatis, L. Tuosto, A. Luster, and A. Hidalgo for critical discussion. The LifeAct-GFP mice were gifts from the F. Sepulveda laboratory (Institut Imagine, Paris, France) and the Ana-Maria Lennon-Duménil laboratory (Institut Curie, Paris, France). We thank M. Bernard and G. Le lay for respective contributions to image processing and data analysis. CXCL11_12 was provided by M. Thelen (Institute for Research in Biomedicine, Bellinzona, Switzerland). CCX771 was provided by ChemoCentryx Inc. We thank A. del Monte Monge and V. Andrés for neutrophil isolation from *Lmna*$^{-/-}$ mice (Centro Nacional de Investigaciones Cardiovasculares Carlos III-CNIC, Madrid, Spain). **Funding:** This research was partly supported by an EMBO short-term fellowship (EMBO STF 609-2016) and an EFIS-IL short-term fellowship to B.C. The project was funded by My First IRP grant (IRP 05/18) to B.C. Additional fundings were secured by the AIRC IG grant no. 16797 to C.L. and the ERC Advance Grant under grant agreement no. 322823 to A.V. M.D. was supported by the Fondation pour la Recherche Médicale (SPF201809007121). This work also received the support of the Association Nationale pour la Recherche (ANR-16-CE13-0009, ANR-20-CE15-0019, and ANR-21-CE17-0050), the Emergences Canceropole (SYNTEC project), and Labex-IPGG (RUN) attributed to P.V., as well as the support of "Institut Pierre-Gilles de Gennes" (laboratoire d'excellence, "Investissements d'avenir" program ANR-10-IDEX-0001-02 PSL and ANR-10-LABX-31). O.G. is supported by the University of Padua under the 2019 STARS Grants programme (iNeurons) and Fondazione Umberto Veronesi. **Author contributions:** B.C. designed and performed most of the experiments, analyzed the data, and interpreted the results. M.D. performed the migration experiments and data analysis during the revision process. F.M. and E.M. helped with neutrophil purifications, chemotaxis/TEM experiments, and immunogold staining. A.C. performed immunofluorescence and helped with the micropillar experiments. L.T. performed and analyzed the adhesion experiments. M.V. microfabricated the micropillars. O.G. contributed to the analysis of nuclear deformability. M.M. performed various experiments during the revision. M.B. performed the analysis of collagen gel pore sizes and gene expression. N.E., C.L., B.M., and M.P. helped to design some experiments and interpret the results. P.V. and A.V. supervised the project. B.C. coordinated the study and provided funds. B.C., P.V., and A.V. wrote the manuscript. **Competing interests:** The authors declare that they have no competing interests. **Data and materials availability:** All data needed to evaluate the conclusions in the paper are present in the paper or the Supplementary Materials.

Submitted 6 July 2021
Accepted 3 November 2022
Published 22 November 2022
10.1126/scisignal.abk2552

Science Signaling

Atypical CXCL12 signaling enhances neutrophil migration by modulating nuclear deformability

Bianca CalìMathieu DeygasFabio MunariElisabetta MarcuzziAntonino CassaráLara ToffaliMassimo VetrallaMathilde BernardMatthieu PielOnelia GaglianoMarta MastrogiovanniCarlo LaudannaNicola ElvassoreBarbara MolonPablo VargasAntonella Viola

Sci. Signal., 15 (761), eabk2552.

Squeezing nuclei and neutrophils through the gap

Neutrophils are innate immune cells that are among the first responders to infection. Chemoattractant molecules called chemokines recruit neutrophils from the circulation to target sites in tissues. Given their large size and relative stiffness, nuclei are the main source of friction as neutrophils squeeze through the confines of the interstitial space. Calì *et al.* found that the chemokine CXCL12, which was previously implicated in stimulating neutrophil migration, increased the deformability of nuclei in primary mouse neutrophils. CXCL12 acted through the atypical receptor ACKR3, leading to PKA-dependent chromatin compaction, thereby facilitating neutrophil movement through restricted microenvironments in vitro—JFF.

View the article online
https://www.science.org/doi/10.1126/scisignal.abk2552
Permissions
https://www.science.org/help/reprints-and-permissions

Science Signaling (ISSN) is published by the American Association for the Advancement of Science. 1200 New York Avenue NW, Washington, DC 20005. The title *Science Signaling* is a registered trademark of AAAS.